DAYANANDA SAGAR COLLEGE OF ENGINEERING

(An Autonomous Institute affiliated to Visvesvaraya Technological University, approved by AICTE & UGC, Accredited by NAAC with 'A' grade and ISO 9001-2015 Certified Institution)

DEPARTMENT OF AERONAUTICAL ENGINEERING

(Accredited by National Board of Accreditation, NBA)

A Project Report on

"ARTICULATION AND ANALYSIS OF SPANWISE ADAPTIVE WING"

Final Year Project (17AE8ICPR2)

Submitted in partial fulfillment for the award of the degree

BACHELOR OF ENGINEERING
in
AERONAUTICAL ENGINEERING

Submitted By

Butani Prince Nileshbhai (1DS17AE009)

Kanagali Jayraj Pramod (1DS17AE019)

Mahek Atul Sanghvi (1DS17AE025)

Vinod Kumar Boyalla (1DS17AE055)

Under the guidance of

Dr. Hareesha N G, M.Tech(CIM), Ph.D (Kinameatics)
Associate Professor [HOD], Department of Aeronautical Engg.
Dayananda Sagar College of Engineering
Bengaluru-560078

2020-21

DAYANANDA SAGAR COLLEGE OF ENGINEERING

(An Autonomous Institute affiliated to Visvesvaraya Technological University, approved by AICTE & UGC, Accredited by NAAC with 'A' grade and ISO 9001-2015 Certified Institution)

DEPARTMENT OF AERONAUTICAL ENGINEERING

(Accredited by National Board of Accreditation, NBA)

CERTIFICATE

Certified that the project work entitled **"Articulation and Analysis of Spanwise Adaptive Wing"** carried out by Mr. **Butani Prince Nileshbhai (1DS17AE009),** Mr. **Kanagali Jayraj Pramod (1DS17AE019),** Mr. **Mahek Atul Sanghvi (1DS17AE025),** Mr. **Vinod Kumar Boyalla (1DS17AE055),** in partial fulfillment for the award of **Bachelor of Engineering** in **Aeronautical Engineering**, during the academic year 2020-21. It is certified that all corrections/suggestions indicated for internal assessment have been incorporated in the report deposited in the departmental library. The project report has been approved as it satisfies the academic requirements in respect of project work prescribed for the said degree.

Signature of the Guide	Signature of the HOD	Signature of the Principal
(Dr. Hareesha N G)	**(Dr. Hareesha N G)**	(**Dr. C P S Prakash**)

Name of the examiners	Signature
1)	
2)	

DECLARATION

We, [Mr. **Butani Prince Nileshbhai (1DS17AE009),** Mr. **Kanagali Jayraj Pramod (1DS17AE019),** Mr. **Mahek Atul Sanghvi (1DS17AE025),** Mr. **Vinod Kumar Boyalla (1DS17AE055)**], hereby declare that this dissertation work entitled **"Articulation and Analysis of Spanwise Adaptive Wing"** has been carried out by us under the guidance of **Dr. Hareesha N G,** Associate Professor [HOD], Department Of Aeronautical Engineering, in partial fulfillment of the requirement of the degree **Bachelor of Engineering in Aeronautical Engineering**.

Place: Bangalore
Date: 9th June 2021

Butani Prince Nileshbhai (1DS17AE009)
Kanagali Jayraj Pramod (1DS17AE019)
Mahek Atul Sanghvi (1DS17AE025)
Vinod Kumar Boyalla (1DS17AE055)

ACKNOWLEDGEMENT

Before introducing our thesis work, we would like to thank the people without whom the success of this thesis would have been only a dream.

We express our deep sense of gratitude and indebtedness to **Dr. Hareesha N G,** Associate Professor [HOD], Department of Aeronautical Engineering, for his valuable guidance, continuous assistance, and in the critical appraisal of the thesis and for providing the facilities required for the completion of this project work.

It is with great pleasure, we extend our gratitude and thanks to **Dr. C P S Prakash**, Principal, Dayananda Sagar College of Engineering, for his encouragement throughout the project.

We are also thankful to **Dr. Srikanth Salyan,** Project coordinator, Department of Aeronautical Engineering for his encouragement in completing this project work.

We feel short words to express our heartfelt thanks to all our family members and friends and all those who have directly or indirectly helped me during our course.

Butani Prince Nileshbhai (1DS17AE009)

Kanagali Jayraj Pramod (1DS17AE019)

Mahek Atul Sanghvi (1DS17AE025)

Vinod Kumar Boyalla (1DS17AE055)

ABSTRACT

Wings are a crucial part of an aircraft as they generate the lift. To generate lift, the airplane must be pushed through the air. There is a resistance of motion through air in the form of aerodynamic drag. Spanwise adaptive wing is a concept wherein during the flight the wings are folded at both ends downwards. This is possible by using different actuator mechanisms like shape memory alloy.

The Spanwise Adaptive Wing (SAW) concept uses a high-force, solid-state Shape Memory Alloy (SMA)-based actuator to create a structurally efficient and reliable method of deflecting a part of the wing in flight. The wings will be fully extended (i.e., without any folding) while take-off to gain maximum lift induced from the wing planform area. After reaching a certain altitude, the wings will be folded downwards to reduce the drag offered by the wings with the help of shape memory alloy or hydraulic mechanism.

The wing is modelled taking some reference airplanes and testing through analysis for the structural, flow and vibrational properties of the wing. The ribs, spars are designed according to the analysis and tested again for avoiding wing failure. Further, the aerodynamic analysis is carried out to compare the drag reduced by the application of the mechanism.

TABLE OF CONTENTS

LIST OF TABLES

LIST OF FIGURES

LIST OF ABBREVIATIONS & NOTATIONS

L	Lift Force
CL	Coefficient of Lift
D	Drag Force
CD	Coefficient of Drag
L/D	Lift to Drag ratio
AoA or α	Angle of Attack
SAW	Spanwise Adaptive Wing
NASA	The National Aeronautics and Space Administration
NiTi	Nickel Titanium
Mf	Martensite Final
As	Austenite Start
Af	Austenite Final
SMA	Shape Memory Alloys
UAV	Unmanned Aerial Vehicle
CFD	Computational Fluid Dynamics

CHAPTER 1

INTRODUCTION

1.1 SPANWISE ADAPTIVE WING

Many researchers have tried to increase the aerodynamic properties by using different mechanisms such as airfoil developments, use of winglets, reduction in weight, and many others.

Spanwise adaptive wing is also one of the developments but has a greater advantage than other developments. Such as

- It helps to increase the lift and reduce drag.
- The efficiency of fuel might be increased.
- The workload on control surfaces reduces especially on rudders.
- In the development of supersonic flight, this concept would be very helpful.

This concept is not new but has lately came into consideration. This concept came from the inspiration of aircraft development i.e., birds. When the birds fly, they try to fold their wings to reach a greater distance without much effort. So, from there the first aircraft to implement was the aircraft XB-70 Valkyrie during the 1960s. NASA has also started to implement this since 2018. The only problem which XB-70 Valkyrie had was its mechanism, which was quite difficult to implement and consumed a lot of weight which use to make it less useful. So, NASA came with this concept again using the mechanism of shape memory alloy which reduced the weight of the wing and is still under research in aircraft like the F-18 unmanned wing as shown in Fig. 1.1.

Fig. 1.1 F-18 aircraft with Spanwise Adaptive Wing

1.2 SHAPE MEMORY ALLOY

A shape-memory alloy is an alloy that can be deformed when cold or low temperature martensite phase but returns to its original shape when heated above the transformation temperature. It is also known as memory alloy, smart metal, memory metal, smart alloy, or muscle wire. Shape memory alloys change from austenite to martensite upon cooling; Mf is the temperature at which the transformation to martensite completes upon cooling. Consequently, during heating AS and Af are the temperatures at which the transition from martensite to austenite starts and finishes. Frequent use of the shape-memory effect may cause to a shift of the characteristic transition temperatures. The highest temperature at which SMAs can no longer be stress-induced is known as MT, in which the shape memory alloys are permanently deformed. The transformation from the martensite phase to the austenite phase is only based on temperature and stress, not time, as most phase changes are, as there is no diffusion involved in it. Similarly, the austenite structure derives its name from steel alloys of a similar structure. It is a reversible diffusion less transformation between these two phases that results in special properties. Although martensite can be created from austenite by rapidly cooling carbon-steel, this operation is not reversible, so steel does not have shape-memory properties.

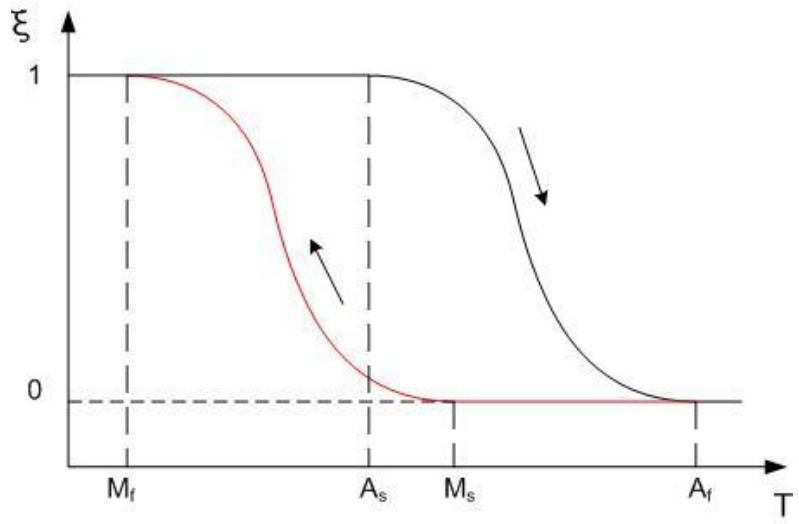

Fig. 1.2 Plot of Martensite function vs Temperature

In Fig 1.2, ξ(T) shows the martensite fraction. The variation between the heating transformation and the cooling transformation leads to hysteresis where some of the mechanical energy is lost in the process. The shape of the curve relies on the material properties of the SMA, namely the alloy's composition and work hardening.

CHAPTER 2

LITERATURE SURVEY

2.1 INTRODUCTION

The intent of this is to provide the details of similar kind of work done by various other people on topics, such as:

a. Spanwise adaptive wing
b. Actuation mechanism in wing
c. Shape memory alloys
d. Airfoil selection
e. Modelling and analysis
f. Wing structural components
g. Stability and control
h. Spar design
i. Material selection for the wing
j. Aspect ratio

2.2 TOPIC-WISE SURVEY

2.2.1 SPANWISE ADAPTIVE WING

The Spanwise adaptive wing is being tested by NASA since 2018 [1]. It is primarily aiming on design and analysis of the SAW with mathematical techniques. An innovative modelling method and the aerodynamic analysis of folding wing-tip UAVs are considered. The concept of SAW is used and tested in subsonic flight speeds in a wind tunnel.

The concept implies folding the aircraft wing end from 0 to 40 degrees. The aim of the project is to obtain a broad spectrum of aerodynamic benefits in flight by folding wings [2]. It also talks about the extra stability benefits it provides to aircraft. The testing is proceeded in UAVs and has taken challenge produced by NASA to the world in the aircraft industry.

2.2.2 ACTUATION MECHANISM IN WING

Early information stating that having reshaping of wings that adjust at various flight velocities can result in improved airplane productivity [3]. Possible points of interest over fixed-wing incorporate augmentation for stability and force for airplane yaw, drag decrease, radar location, and airplane security.

The latest development in SMA activation innovation requires detailed examination on cruise flight wing collapsing for airplanes in which the wing dimensions are very low for regular frameworks. Otto Lilienthal was the first person in the 1800s to lay aviation trails [4].

The camber and a suitable thickness of the airfoil improved aerodynamic performance when contrasted with a level plate. A variable span wing is a trade-off between the performance and mobility qualities of enormous aspect ratio and low aspect ratio wings, as the wing length is changed by the mission prerequisites. Hypothetically, expanding the wingspan and wing area diminishes the spanwise lift distribution for a similar lift. Subsequently, the wing drag could be decreased, and thus, the range and endurance of the airplane [5].

A two degree-of-freedom (DOF) mechanism which is designed and fabricated that is appropriate for morphing wing applications. The numerical results of the model simulation are verified against the experimental results using a test setup to validate the proposed model prediction. The proposed mechanism is fabricated in order to verify the model with experimental data [6].

This study performed Experiments were conducted under wind tunnel conditions to verify analysis and to investigate the effects of its application on the aerodynamic behavior of the wing. A number of experiments were conducted to investigate the feasibility of wing morphing using Shape memory alloy [7].

Various wing morphing development used by various authors which are compared and perform some structural testing to prove the capabilities of the shape memory alloy actuated truss beam and examine the various SMA actuation capabilities in meeting some desired shape for any application. It also displays the progress, challenges, and developments which is carried on till date [8].

2.2.3 SHAPE MEMORY ALLOYS

The characteristics of shape memory alloys extend greatly over the temperature range covering their transformation [9]. Two-way shape memory effect is a property of shape

memory alloys i.e.; shape of the material changes on both heating and cooling. To obtain this two- way shape memory aftereffect different heat treatment and mechanical training processes have been suggested to introduce two-way shape memory effect.

Excess nickel strongly depresses the transformation temperature and increases the yield strength of the austenite. The discovery of shape memory alloys can be dated back to the early 1950s, but the engineering importance of shape memory alloys was not well identified until the shape memory effect was discovered in NiTi alloys [10]. It is necessary to know that the actuation rates of the NiTiHf alloy are considerably higher than those of conventional NiTi because the martensite finish temperature is near 100℃, well above ambient temperatures and therefore increasing cooling rates.

2.2.4 AIRFOIL SELECTION

The research is towards the Unmanned aerial Vehicle's airfoil selection. The Airfoil database has thousands of airfoils to choose which makes it very difficult to select among them. As moving towards applications of the research as UAV the requirement of lift is quite low as the altitude it should fly is very less compared to the Aircrafts [11]. It uses XFLR5, Java Foil, X-foil tools to determine their aerodynamic characteristics and aerodynamic plots used as a base for every aircraft design.

2.2.5 MODELLING AND ANALYSIS

The modelling and analysis of the wing is performed using CATIA V5 and ANSYS workbench. Analysis is performed on the wing by fixing the root chord of the wing , leaving the tip chord at the free end. For validation a procedure was performed using ANSYS workbench and an FEA software [12].

2.2.6 WING STRUCTURAL COMPONENTS

Ribs are those elements in the wings structure that are usually made up of wood, metal, plastic, composite. Ribs are attached to the spar. The aim of the present work is to calculate the resonance of the machine components to obviate the critical vibrations that leads to deformation. Before the fabrication of model, the FEM analysis is done. A continuous quantity like displacements, temperatures, pressure, which can be estimated by a discrete model which is defined over a finite number of sub-domains [13].

In the analysis, the simplified wing geometry is gathered so that it will reduce the complexity of the analysis. The vibrational analysis is used for getting the mode shapes of bending, Ansys workbench is used as the structural analysis tool [14].

A progressive method was employed to characterize and analyze the dynamic aeroelastic attributes of the TDT model. A purely analytic procedure was used to display positive flutter margin results at the Model Systems Review. The modelled TDT structure had higher stiffness than the actual model which we know after detailed inspection. Therefore, it required to perform some extra flutter margin checks [15]. It has gains from developments in spine modelling, aerodynamic and automated structural by aeroelastic characterization.

2.2.7 STABILITY AND CONTROL

For any design process the first step is the sizing of the main components. The characteristics of Stability and control are used for assistance in the design process. The software allows the stability and control analysis of the aerodynamics set generated using CFD tools, aero-structural sizing, and geometry for low-speed flights and high-speed flights. The stability co-efficient for conceptual designs are obtained from the stability analysis results [16].

In Aircraft design concentrates on the design of the wing and its stability and the problems dealing with stability. Evidently, we know the wing produces lift force to counter the weight of the aircraft along with drag force and pitching moment. So, adding all forces and moments applied on aircraft about the COG (Centre of gravity) is zero then the aircraft is in stable or trim condition. Therefore, the aircraft wing configuration has great importance to its aerodynamic efficiency and characteristics [17].

2.2.8 SPAR DESIGN

Spar is the main-load (bending) carrying members in the wing along the spanwise direction. It mainly focusses on the prototype design of an aircraft spar beam to increase the structural properties without compromising on its strength or load carrying capability. The spar with cut-out and without cut-out is modelled and the static structural analysis is performed with appropriate forces, then visualize the deformation and frequency modes. This paper results that tapered spar with cut-out at minimum stress region offers reduction in weight with structural efficiency. The dimensions for the I -section are referred from this article [18].

2.2.9 MATERIALS SELECTION FOR THE WING

The design of aircraft wing is the most important part. Some important factor to be considered for selection of material is its lightweight without compromising on the required strength. The materials employed for the ribs, spar and skin are Aluminium 2024-T3, Aluminium 7075-T651 and carbon epoxy. The advantage of using carbon epoxy reduces weight of the wing and serves as a replacement for Aluminium [19].

2.2.10 ASPECT RATIO SELECTION

Aspect Ratio has always been an important factor in designs, for several reasons, but, it's even more important in gliders than in powered craft. Another effect of aspect ratio on the aircraft performance is how it affects the plane's roll rate. The higher the aspect ratio is, the slower the roll rate will be. Depending on the mission profile that the aircraft is intended to fulfil, a designer chooses a suitable aspect ratio, tabulates the aspect ratios for different types of aircrafts [20]. The factor of safety and structural loads limit has been understood [21].

2.3 GAP IN LITERATURE SURVEY

- The concept of SAW was a challenge given by NASA to the entire world for the aircraft industry but no one has tried to find the benefits it might lead to.
- The concept involved the folding of wings but no research has been made regarding the aerodynamic advantages at higher subsonic speeds after producing this concept.
- There has not been any research on transient or dynamic analysis over SAW.
- In research of spanwise adaptive wing use of flaps and other high lift devices has not been discussed so far.

2.4 PROBLEM STATEMENT

At higher subsonic speeds, the drag force increases drastically in aircraft which confines our application. Using the concept of a spanwise adaptive wing with the help of shape memory alloy producing a highly stable, fuel-efficient, and even applicable for higher speeds.

2.5 OBJECTIVES

1. Finding some best airfoils and selecting best one based on analyses in XFLR5 and ANSYS.
2. Performing calculation for wing design and modelling the wing using CAD software.
3. Modelling of mechanism using shape memory alloy to apply the concept of spanwise adaptive wing.
4. Performing structural analysis for the wing and for material selection.
5. Performing modal, CFD and transient analysis and comparing the results.

2.6 SUMMARY

Using the various literature survey, the concept of the spanwise adaptive wing has been understood and the actuation required for it to take place has been studied. The material shape memory alloys working is also understood which can be an idea to provide a new actuation mechanism for the SAW. The airfoil selection procedure, Modelling, and analysis used for a similar type of concept known as morphing wing are studied. Finally, for any wing to be used the stability required is also been studied.

CHAPTER 3

METHODOLOGY

3.1 BRIEF PROCEDURE

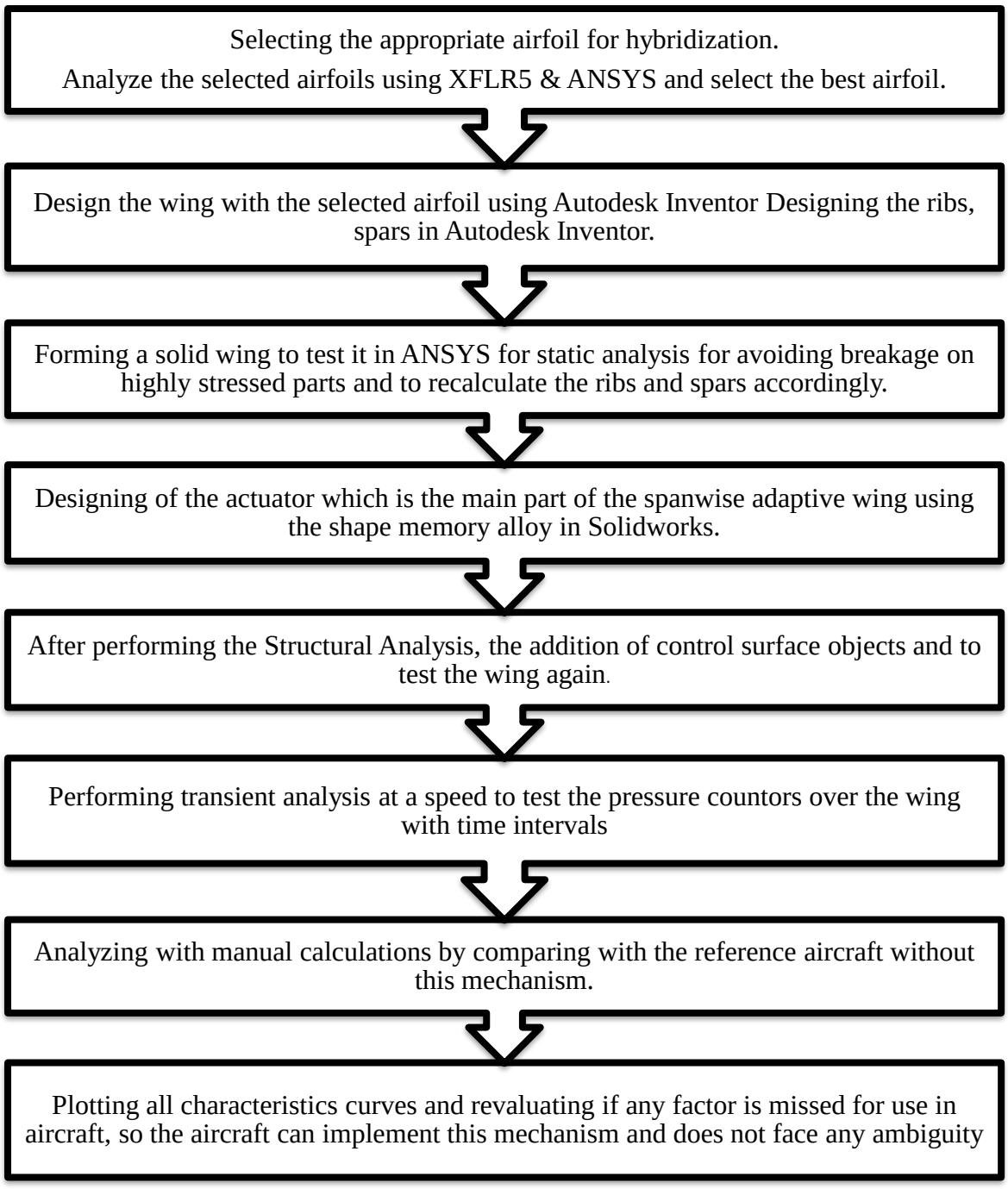

Fig. 3.1 Flowchart of methodology

Fig. 3.1 depicts a flowchart to show entire process of methodology that will be adopted throughout the entire project work to obtain the objectives.

3.2 AIRFOIL SELECTION

To choose the airfoil that suits the application of spanwise adaptive wing some reference is needed to be known. From the airfoil data, these best three airfoils were chosen:

- E387
- Clark-Y
- SD7037

3.2.1 PLOTTING USING XFLR

By plotting the coordinates of the airfoils in XFLR, and taking the boundary conditions as given below, the lift, drag, and lift-to-drag ratio of the three airfoils were observed closely.

- Reynold's Number Range: 1,00,000 to 8,00,000
- The angle of Attack(α): -5º to 15º

3.2.1.1 E387 AIRFOIL:

The Fig. 3.2 of the airfoil analysis, the lift increases almost linearly with increase in angle of attack, and after a certain point, it starts decreasing. The angle of attack at this point of co-efficient of lift (CL) is called a stall angle. A stall in an aircraft arises when the angle of attack of an airfoil go beyond the value which creates a maximum lift as a result of airflow across it, which is around 14º.

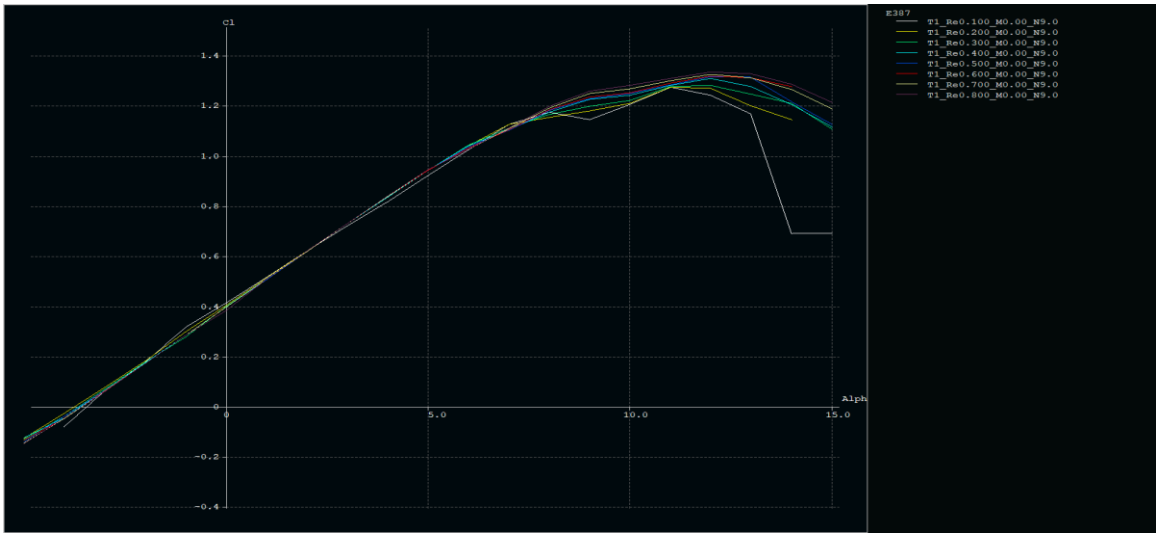

Fig. 3.2 Plot of CL Vs α for the E387 airfoil

In Fig. 3.3 the drag increases exponentially with increase in angle of attack. In Fig. 3.4 the lift-to-drag (L/D) ratio graph is plotted for a better understanding of the airfoil and its selection. The L/D ratio suggests which airfoil has better lift compared to the drag for the given angle of attack.

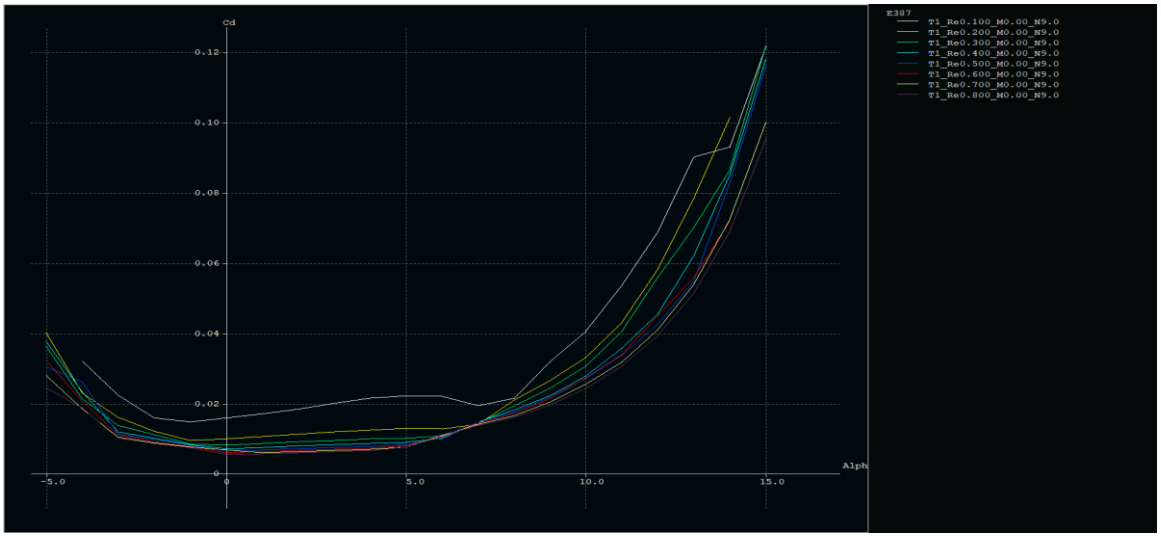

Fig. 3.3 Plot of CD Vs α for E387 airfoil

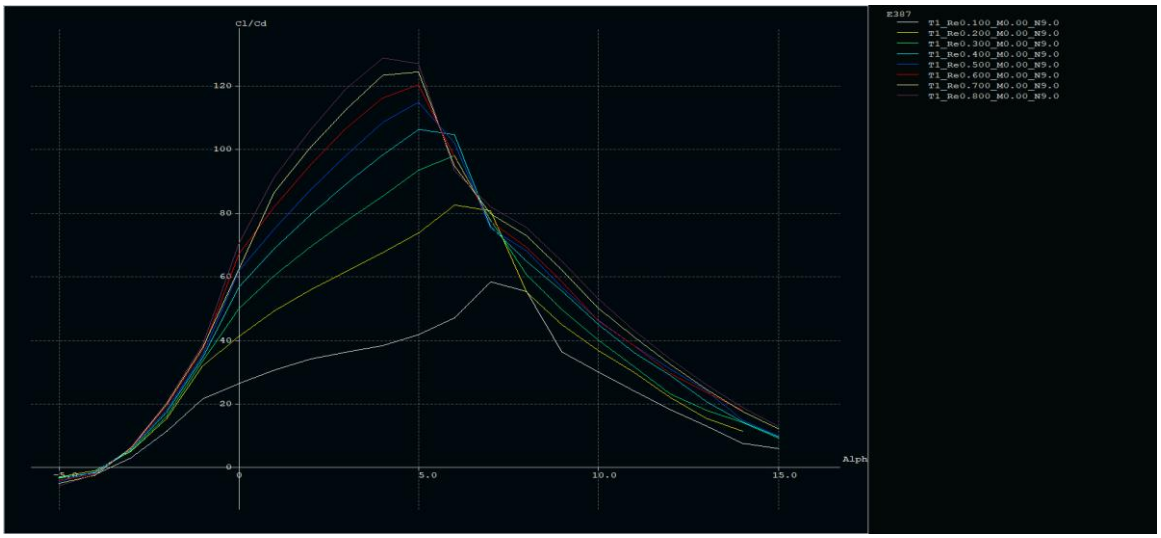

Fig. 3.4 Plot of CL/CD Vs α for E387 airfoil

3.2.1.2 CLARK-Y AIRFOIL:

The Fig. 3.5 of the airfoil analysis, the coefficient of lift increases almost linearly with the increase in the angle of attack, and after a certain point, it starts decreasing. The angle of attack at this point of co-efficient of lift (CL) is called a stall angle. In Fig. 3.6 the coefficient of drag increases exponentially with an increase in the angle of attack.

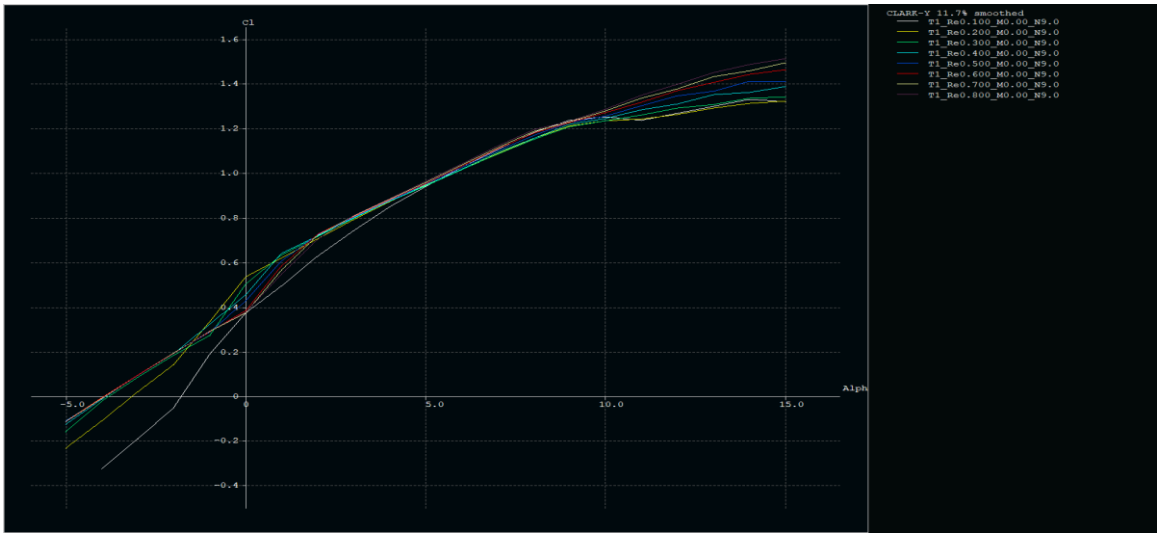

Fig. 3.5 Plot of CL Vs α for Clark-Y airfoil

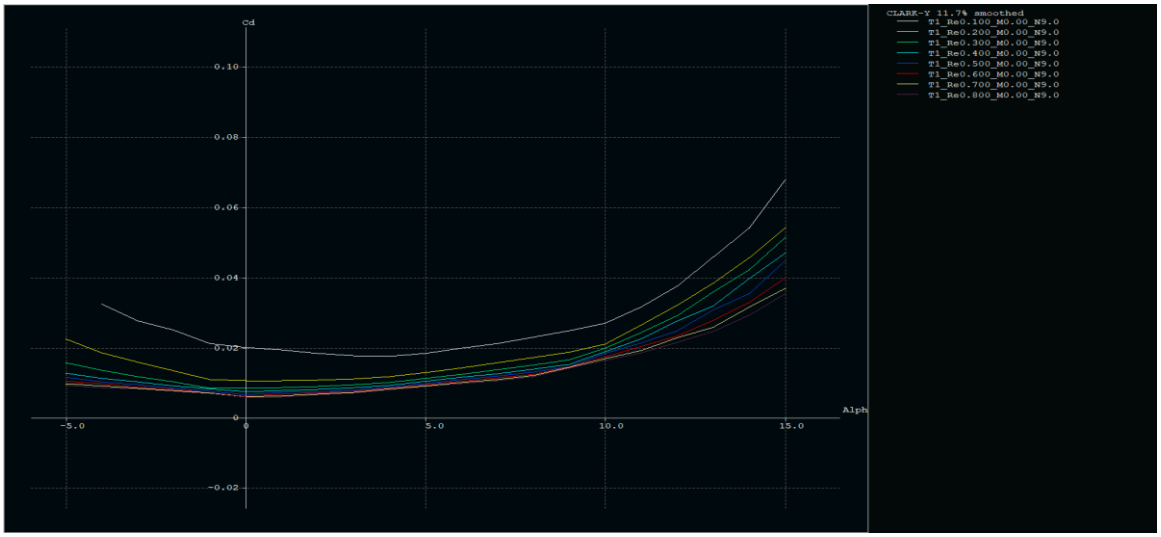

Fig. 3.6 Plot of CD Vs α for Clark-Y airfoil

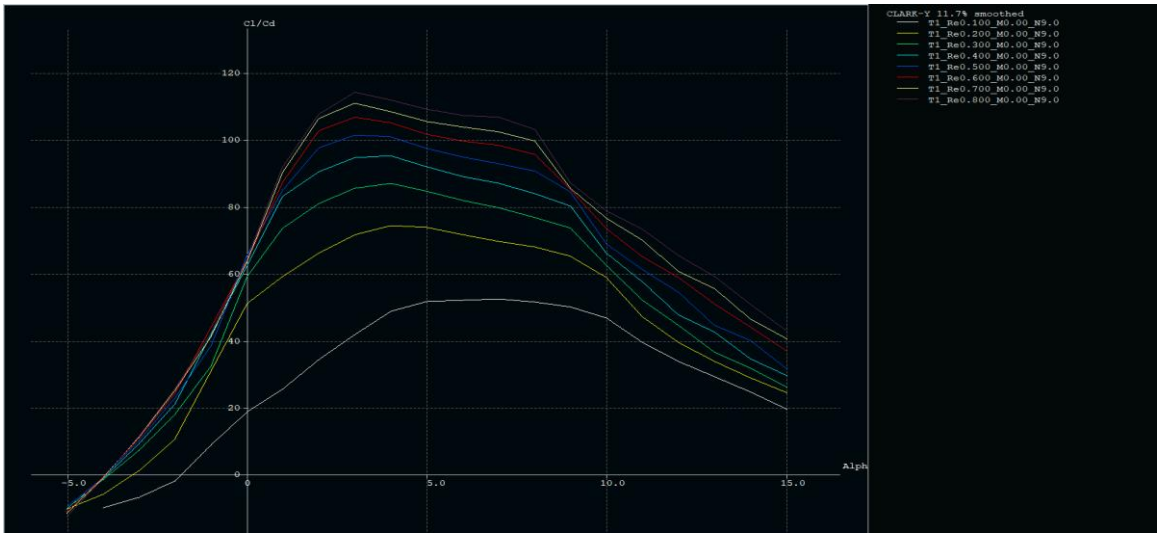

Fig. 3.7 Plot of CL/CD Vs α for Clark-Y airfoil

In Fig. 3.7 the lift-to-drag (L/D) ratio graph is plotted for a better understanding of the airfoil and its selection. The L/D ratio suggests which airfoil has better lift compared to the drag for the given angle of attack.

3.2.1.3 SD7037 AIRFOIL:

The Fig. 3.8 of the airfoil analysis, the coefficient of lift increases almost linearly with the increase in the angle of attack, and after a certain point, it starts decreasing. The angle of attack at this point of co-efficient of lift (CL) is called a stall angle. A stall in an aircraft arises when the angle of attack of an airfoil go beyond the value which creates a maximum lift as a result of airflow across it. This angle changes very little when compared to the cross-section of the airfoil and is generally around 15°. In Fig. 3.9 the coefficient of drag increases exponentially with an increase in the angle of attack.

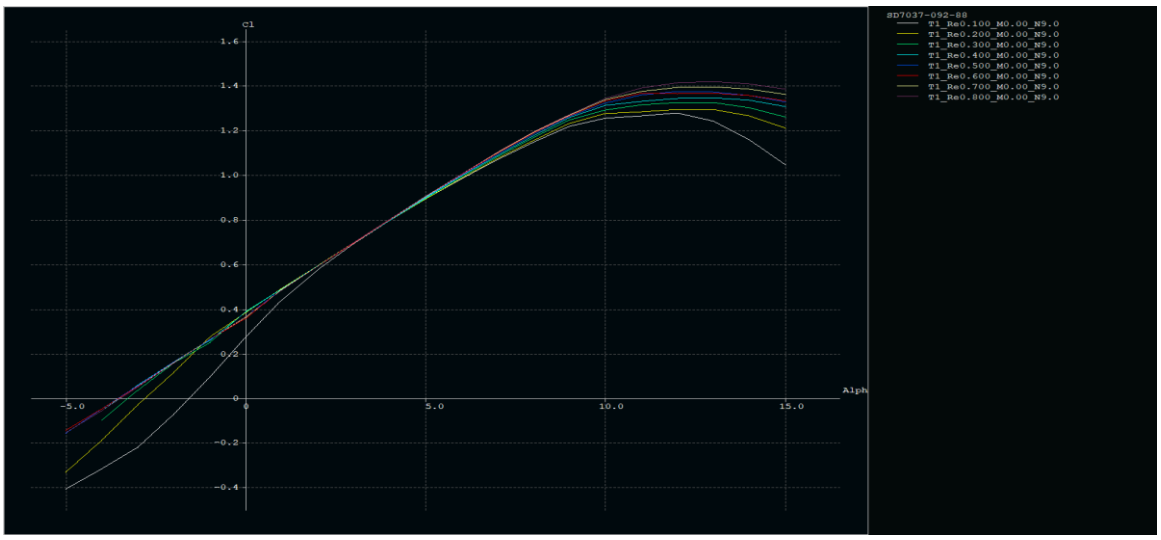

Fig. 3.8 Plot of CL Vs α for SD7037 airfoil

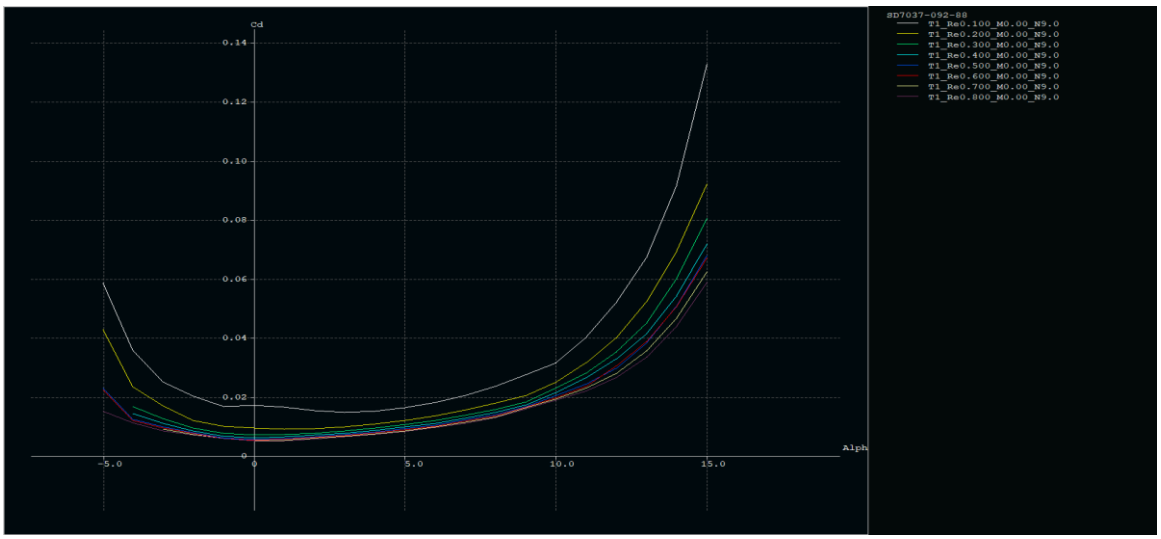

Fig. 3.9 Plot of CD Vs α for SD7037 airfoil

In Fig. 3.10 the lift-to-drag (L/D) ratio graph is plotted for a better understanding of the airfoil and its selection. The L/D ratio suggests which airfoil has better lift compared to the drag for the given angle of attack.

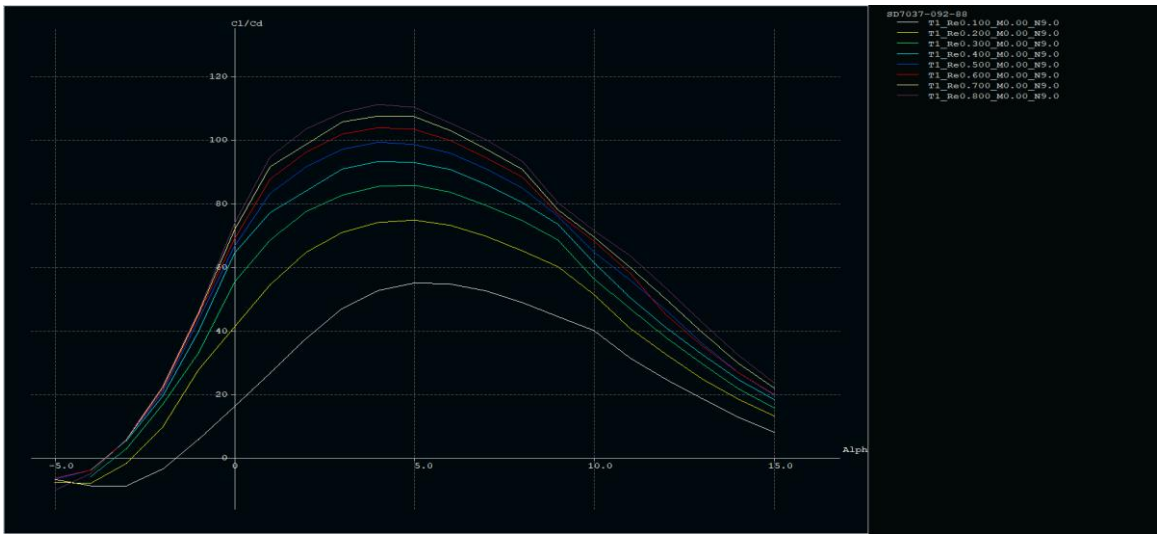

Fig. 3.10 Plot of CL/CD Vs α for SD7037 airfoil

3.2.2 CFD ANALYSIS OVER THE AIRFOILS

To verify the results of XFLR5 and to get lift, drag and the changes with respect to angle of attack and velocity it has been analyzed using the same airfoils using the analysis tool ANSYS.

3.2.2.1 MESHING

MESH PROPERTIES AND BOUNDARY CONDITIONS:

1. Unstructured Mesh

- Meshing method: All Triangles method
- Edge sizing: 500 divisions
- Mesh Refinement: 2

Fig. 3.11 shows the unstructured mesh over the entire airfoil with the domain.

2. Structured Mesh

- Inlet edges division: 50
- Wall: No-slip wall and 100 edge divisions
- Outlet edge division: 50 divisions
- Meshing type: Structured mesh by using face meshing

Fig. 3.12 shows the structured mesh over the entire airfoil with the domain.

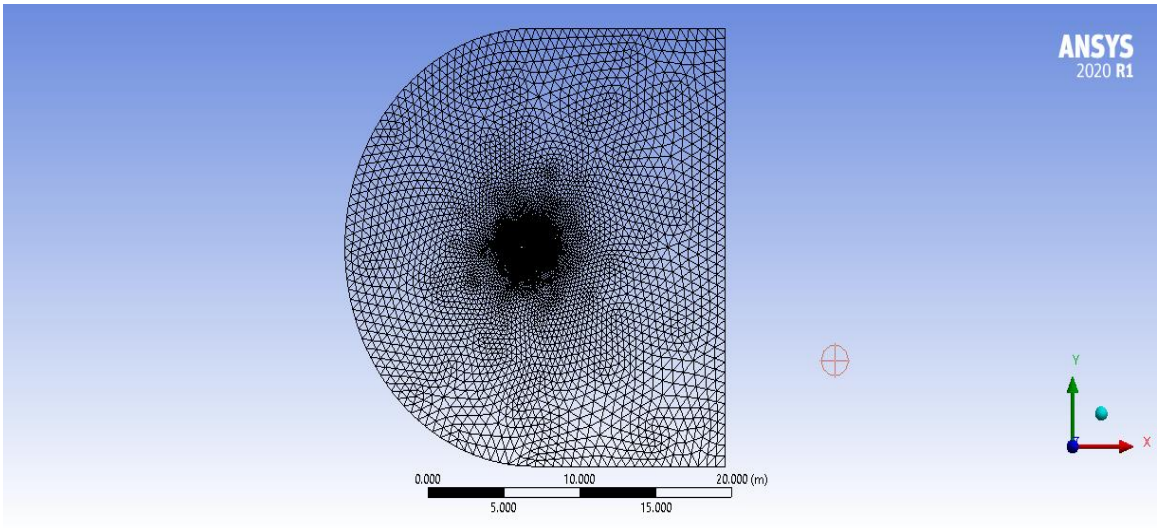

Fig. 3.11 Unstructured mesh over an airfoil

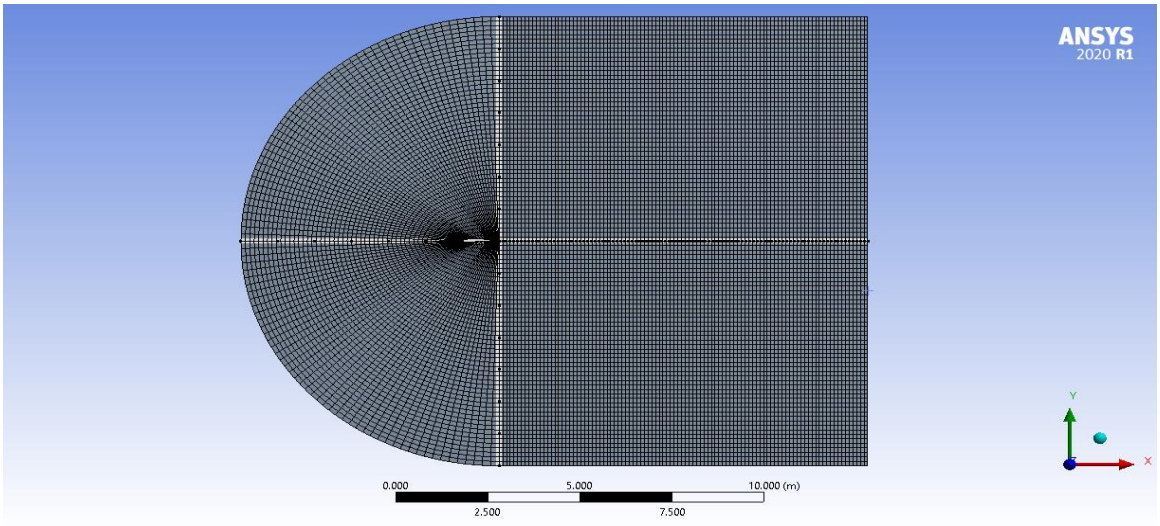

Fig. 3.12 Structured mesh over an airfoil

3.2.2.2 GRID INDEPENDENCE STUDY FOR AIRFOILS

The grid independence study shows that the lift generated for the airfoil is 601.32 N with coarse meshing (Nodes: 15202, Elements: 14830) as in Fig. 3.12, while it is 631.27 N for medium meshing (Nodes: 15469, Elements: 15062) as in Fig. 3.13 and 633.1 N for fine meshing (Nodes: 15569, Elements: 15112) as in Fig 3.14. Thus, the difference between the coarse and medium mesh is in a good amount and thus coarse mesh should not be used here. The difference between a medium-mesh and a fine mesh is very little and thus to avoid the unnecessary increase in computational time, medium meshing is selected (i.e., Nodes: 15469, Elements: 15062).

Grid convergence is the name used to illustrate the improvement of results by using successive finer grids for the calculations. A calculation should move nearer to the correct

answer as the mesh turn into finer, therefore the term grid convergence. Grid dependency study is an essential part of the computational exercise by which discretization error can be minimized to get consistent and stable values. A grid dependency study was done to ensure that the solution does not depend upon the grid quality and the grid size.

In Fig. 3.13 the fine relevance meshing gives the more precise results for the lift generated. As the relevance of the meshing is increased the number of elements increases and the results obtained get better and more accurate. Thus, the difference between the coarse and medium mesh is in a good amount and thus coarse mesh should not be used here.

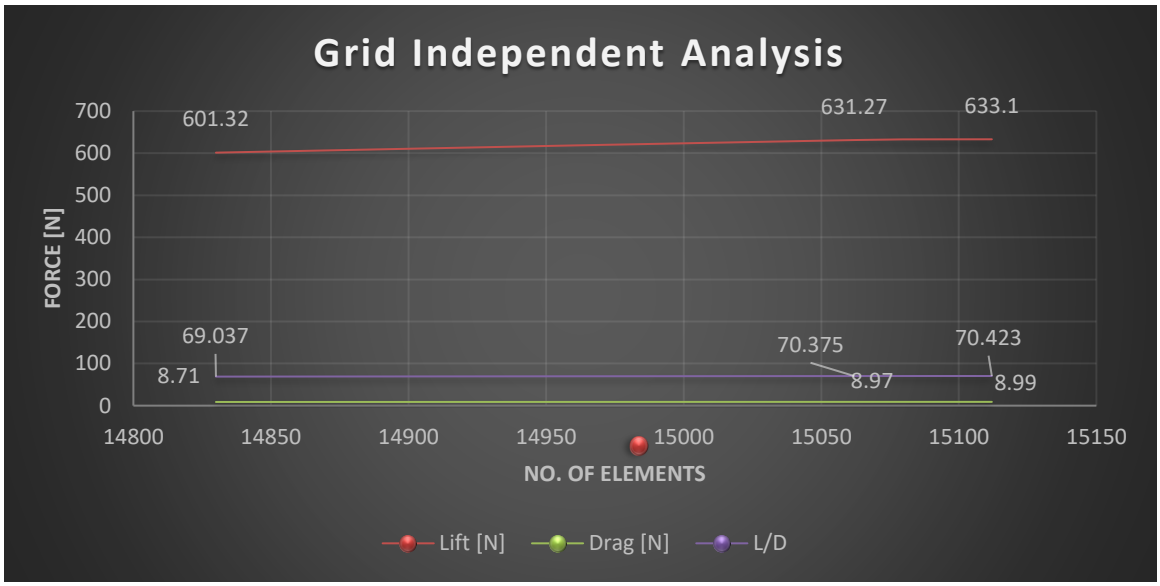

Fig. 3.13 Independent grid analysis

3.2.2.3 CFD ANALYSIS OVER AIRFOILS

This analysis is required for finding the lift and drag performance at various velocities inputted. The parameters for the analysis of the airfoils were:

- The angle of Attack [α]: -5º, 0º, 5º, 10º, 12º

The Reynolds number was taken minimum and based on the following parameters:

The expression for Reynold's Number is given by:

$$R_e = \frac{\rho \times V \times d}{\mu} = \frac{V \times d}{v} \quad (1)$$

Where v = kinematic viscosity (m^2/s)

V = Velocity (m/s)

d = Chord width of airfoil (m)

μ = Dynamic Viscosity (kg/ms)

ρ = Density (kg/m^3)

Eq. 1 represents the formula for calculation Reynold's number which in turn predicts the type of flow. For Reynold's number greater 4000 depicts turbulent flow, below 2000 depicts laminar flow and in between depicts a mixed flow of laminar and turbulence.

For minimum,

Chord width = 0.1 m

Velocity = 15 m/s

Kinematic Viscosity = $1.5111 \times 10^{-5}\ \frac{m^2}{s}$

$$\therefore R_e = \frac{V \times d}{v} = \frac{15 \times 0.1}{1.5111 \times 10^{-5}} = 99{,}265$$

For middle range,

Chord width = 0.1 m

Velocity = 35 m/s

Kinematic Viscosity = $1.5111 \times 10^{-5}\ \frac{m^2}{s}$

$$\therefore R_e = \frac{V \times d}{v} = \frac{25 \times 0.1}{1.5111 \times 10^{-5}} = 2{,}31{,}619$$

For maximum,

Chord width = 0.1 m

Velocity = 55 m/s

Kinematic Viscosity = $1.5111 \times 10^{-5}\ \frac{m^2}{s}$

$$\therefore R_e = \frac{V \times d}{v} = \frac{55 \times 0.1}{1.5111 \times 10^{-5}} = 3{,}63{,}973$$

Fig. 3.14 depicts the flow over the airfoil which performed using ANSYS.

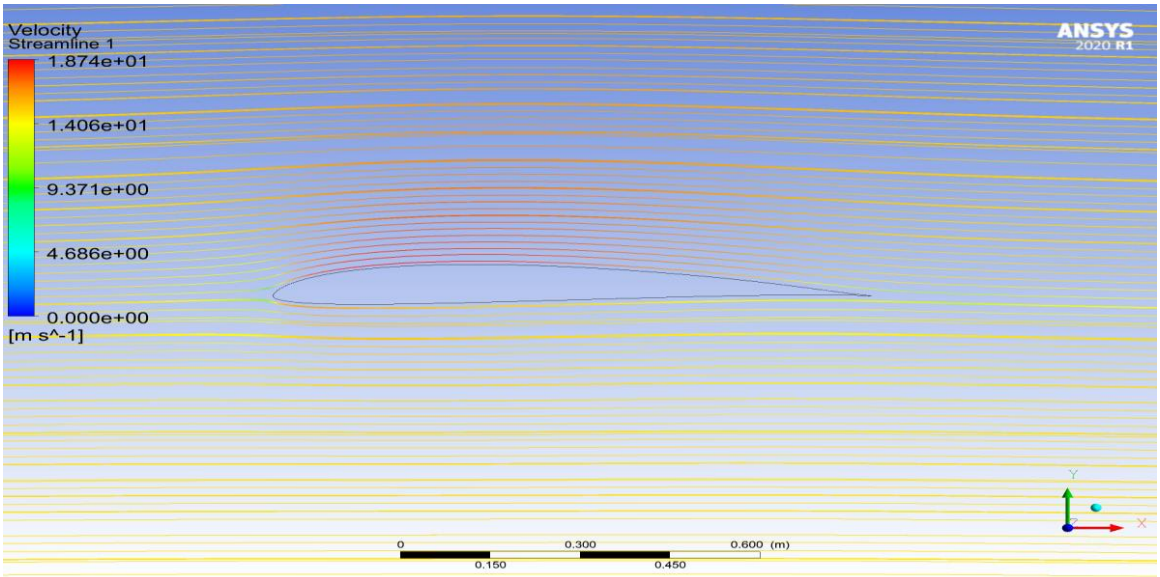

Fig. 3.14 Velocity flow over an airfoil

3.3 DESIGNING OF THE WING

3.3.1 CALCULATIONS OF WING PARAMETERS

Formulas:

1. Area (S) = c×b (in m^2) (2)
2. Aspect ratio (AR) = $\frac{b^2}{S}$ (3)
3. Distance of spar from LE = $\frac{c}{4}$ (4)

Where, Total length of the wing (b) = 9000 mm

Chord length (c)= 1500 mm

Eq. 2 depicts the formula to calculate the planform area of the wing. Eq. 3 depicts the formula to calculate the aspect ratio for a particular wing. Eq. 4 depicts the formula to find out the distance between spar and the leading edge of the wing.

- **Area**

Area =c(chord length) × b(full wing)

Area = 1500 mm×9000 mm

Area = 1,35,00,000 mm^2

Area (full wing) = 13.5 m^2

- **Aspect ratio**

To calculate aspect ratio, considering the full wing span length and wing area.

Aspect ratio =$\frac{b^2}{S}$ = $\frac{9^2}{13.5}$ = 6

Therefore, the obtained aspect ratio = 6 is feasible for wing designing.

- **Spar calculation**

Maximum thickness = 9.2% at 26.1% of chord.

= 0.092×1500 = 138 mm at 26.1% of chord from LE.

Distance of spar from LE = $\frac{c}{4}$ = $\frac{1500}{4}$= 375 mm

Therefore, the spar is been designed at the quarter chord from the leading edge of the airfoil.

- **To calculate distance between two ribs**

Thickness of the rib = 30 mm

Distance between two ribs = 375 mm

Total length of wing (half) from root to tip = 4500 mm

Number of parts in the wing = $\frac{4500}{375}$ = 12 parts

Therefore, for 12 parts 13 ribs need to be placed.

3.3.2 MODELLING OF THE WING USING CAD SOFTWARE

The entire CAD model of the wing has been designed using Autodesk Inventor. CAD model provides the exact view of the real wing with exact dimension given to it.

Fig. 3.15 depicts the dimensions used for the half wing with ribs and spars location from the ends of wing. Fig. 3.16 depicts the CAD model of the wing with skin. Fig. 3.17 depicts the CAD model of the wing with ribs and spars. The number of the ribs and spars and also the wing parameters has been calculated earlier in this project in section 3.3.1 named calculations of wing parameters.

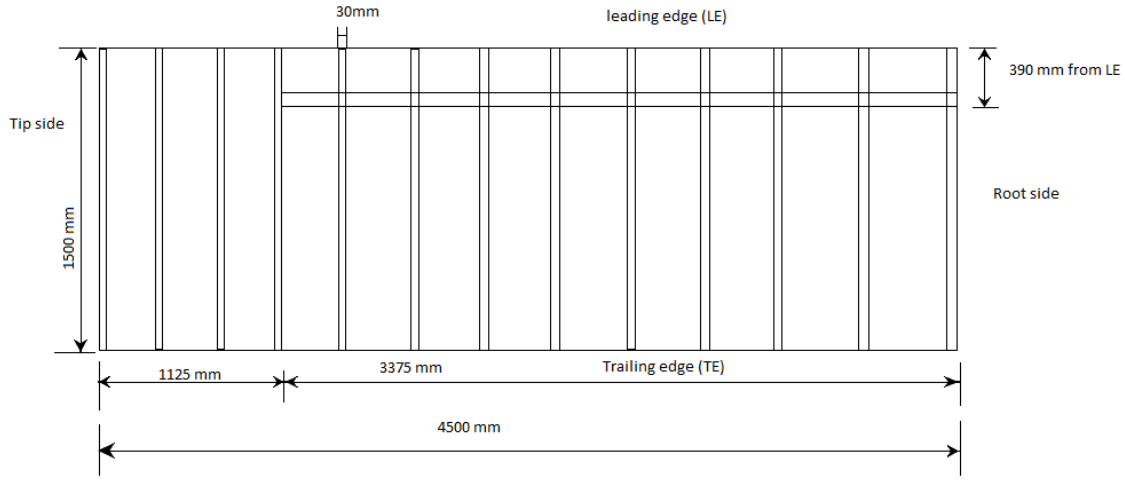

Fig. 3.15 Dimensions of half wing modeled

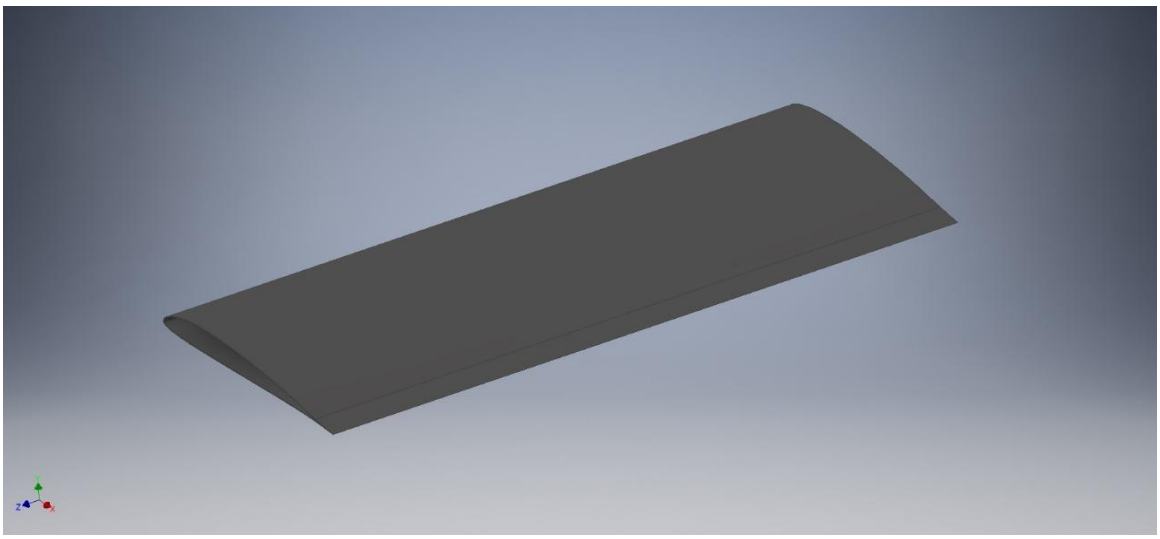

Fig. 3.16 CAD model of the wing with skin

Fig. 3.17 CAD model of the wing with ribs and spars

Fig. 3.18 depicts the cross section used for the I-section. Fig. 3.19 depicts the cross-section used for the C-section.

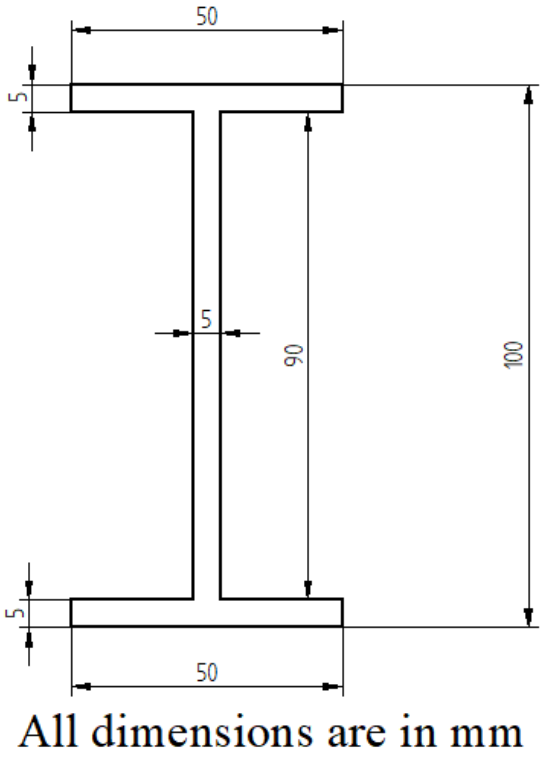

Fig. 3.18 Dimensions of I-section spar

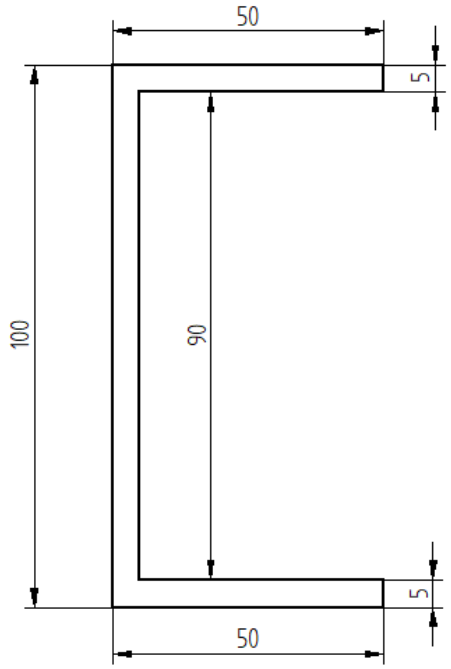

Fig. 3.19 Dimensions of C-section spar

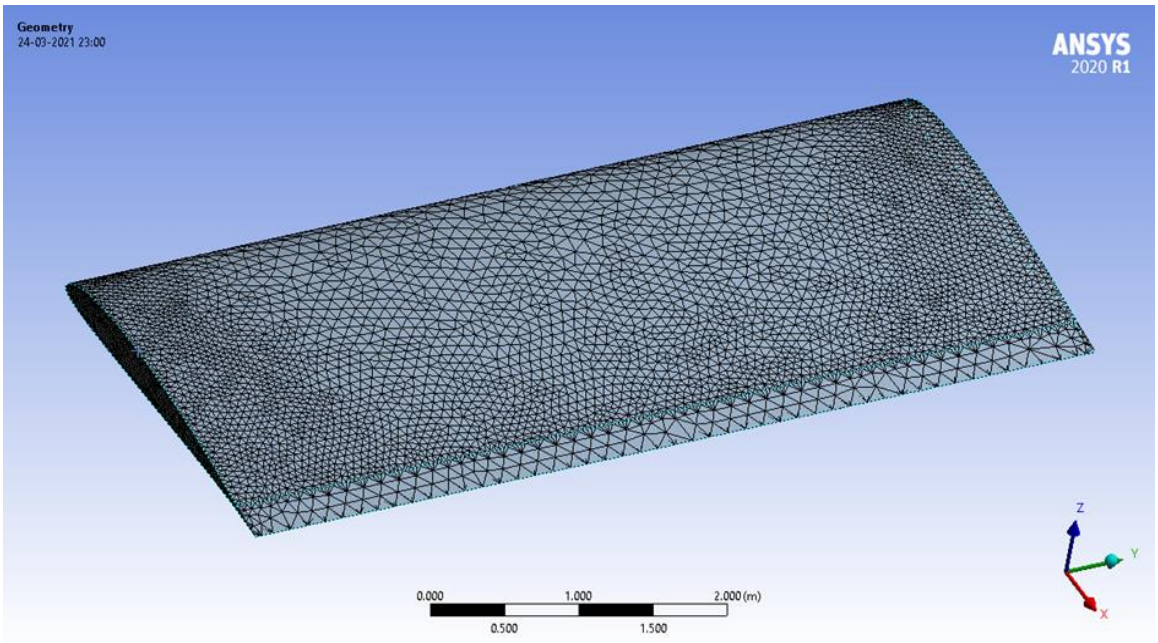

Fig. 3.20 Meshing of the wing

Fig. 3.20 shows the mesh applied to the wing for analysis purpose. Now after modelling the aircraft wing the wing is to be analyzed in structural, modal and flow analyses to compare the results with spanwise adaptive wing designed.

3.3.3 MODELLING OF THE MECHANISM

The mechanism contained a moving top platform, base fixed platform, and 6 linear actuators, allowing movements in 3 independent location coordinates and three independent rotational coordinates (pitch, yaw, and roll). Because it has accurate positioning capabilities, this mechanism is appropriate for the spanwise adaptive wing application. To fold the structures in two independent directions (pitch and yaw), the conceptual design of the planned mechanism uses 2 SMA material. To contract each leg and produce the desired position of the moving platform, the mechanism uses SMA material. Universal joints are used to connect these actuators to two airfoils. To offer opposing moments and adding translational stiffness to the mechanism, two bars are fixed to each plane. The mechanism contains two airfoil plates linked to each other through a universal two degrees of freedom joint. Two separate DOFs are provided by two SMA wires. As most SMA actuators move in one direction (generally, in tension), in this mechanism two springs are used. When the SMA actuators are inactive, these springs tend the mechanism to return to its original position. Each Degree of Freedom's workspace is based on the geometry of the airfoil plates, the SMA length, and the attachment points of the SMA wires to the mechanism. Position sensors implanted in the joints of the mechanism offer angular sensory data. Every rotary degree of freedom uses separate slippery bearing to produce a firm rigidity. The mechanism is linked to each other employing a docking mechanism made up of pins and a set of screws. The mechanism is designed so that two directions of rotation are entirely independent of each other. The motion will be produced in just one direction when one of the SMA actuators is active, because of the design of the mechanism. Therefore, these two degrees of freedom mechanism contain two independent one degree of freedom mechanisms. The planned mechanism can be used in a spanwise adaptive wing by employing it between adjacent sections to form large deformations. The wing can gull and sweep by choosing the length among the sections. This is an effective mixture of movements because it can enhance maneuverability, speed range, and loiter capability of the aircraft. A model of the unit section of the planned mechanism was modeled with each section confined by a rib panel to a rigid airfoil. A similar can be done by using 2 airfoils to actuate through this mechanism. Because of the DOF(Degree of Freedom) of the mechanism that can be possibly accomplished by each section, it is projected that it is unnecessary to have three of these sections to actuate it to the large deformation modes in a wing.

Fig. 3.21 represents the shape memory alloy spring assembly which holds the entire folding mechanism. Contraction and expansion of this spring leads to movement of the mechanism and resulting to perform spanwise adaptive wing concept. Fig. 3.22 represents the bolt used to join these components into a particular form. Fig. 3.23 and Fig. 3.24 represents the support system to the spring of shape memory alloy and to hold both the parts of wing rib. Fig. 3.25 represents the assembled components of the mechanism.

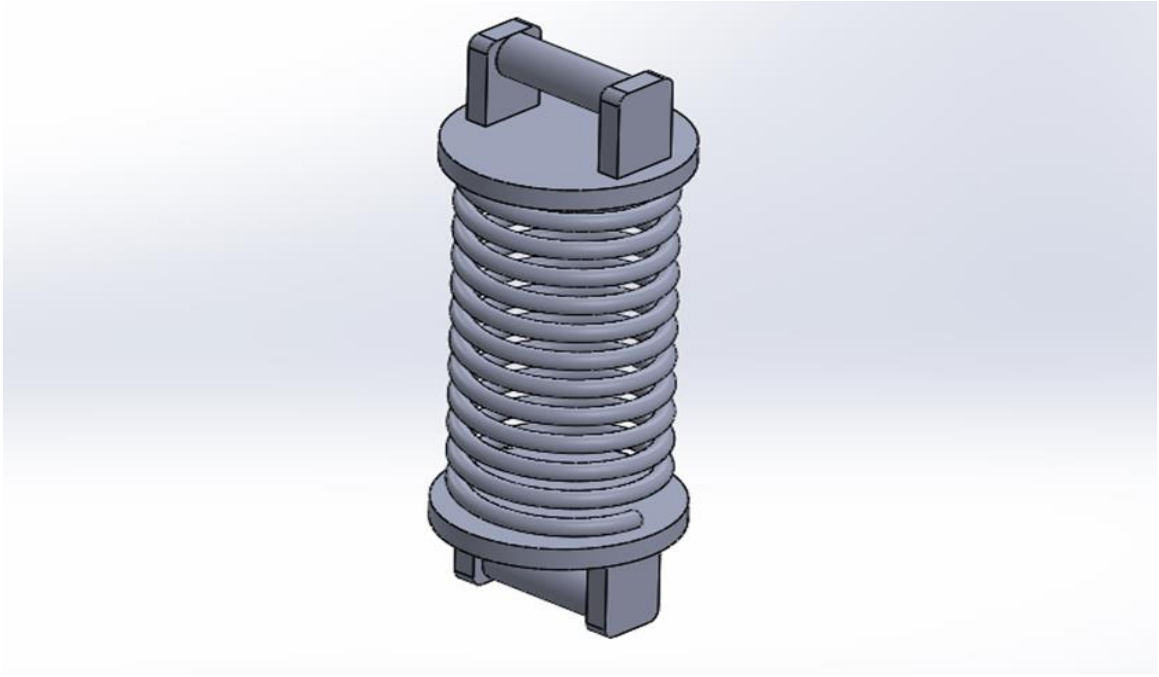

Fig. 3.21 Spring made of shape memory alloy

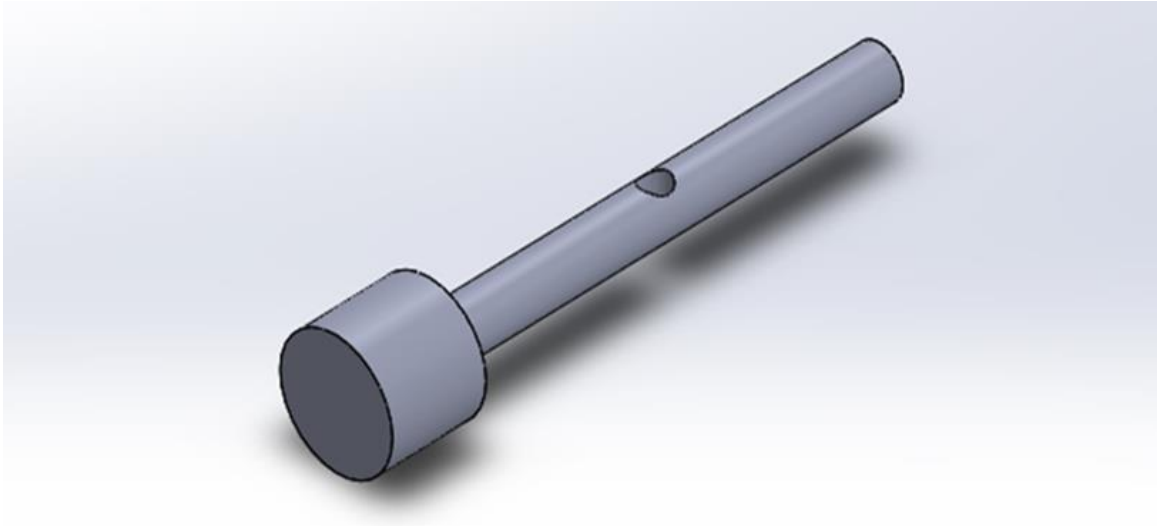

Fig. 3.22 Bolt of the mechanism

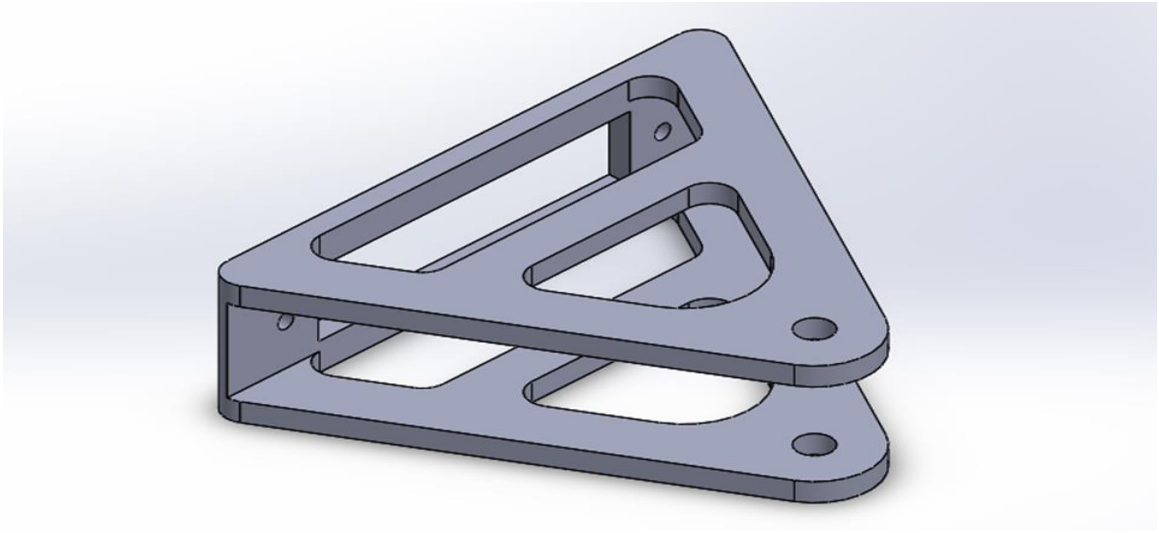

Fig. 3.23 First support of the mechanism

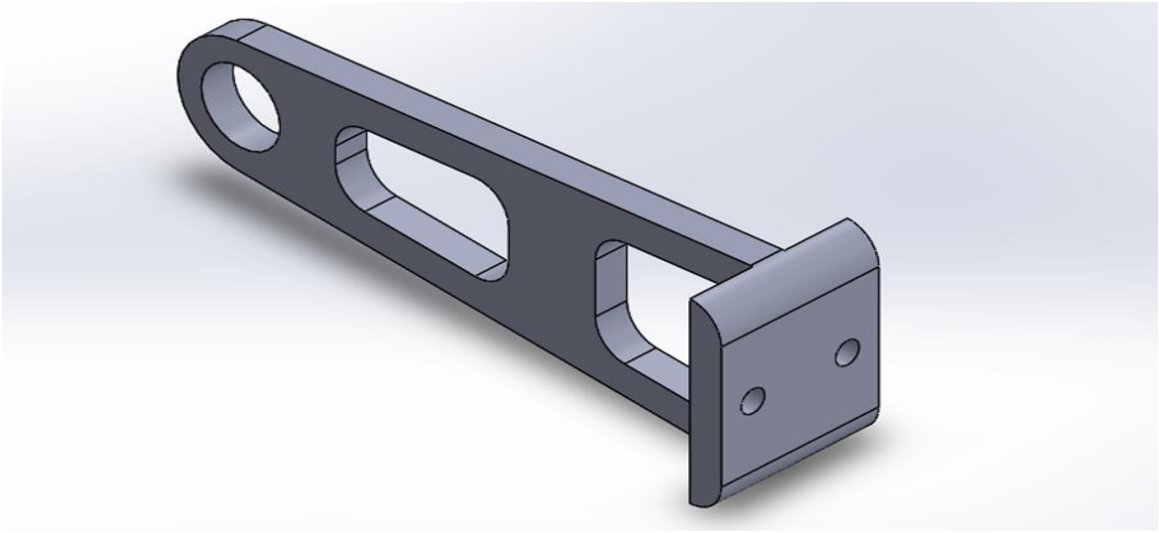

Fig. 3.24 Second support of the mechanism

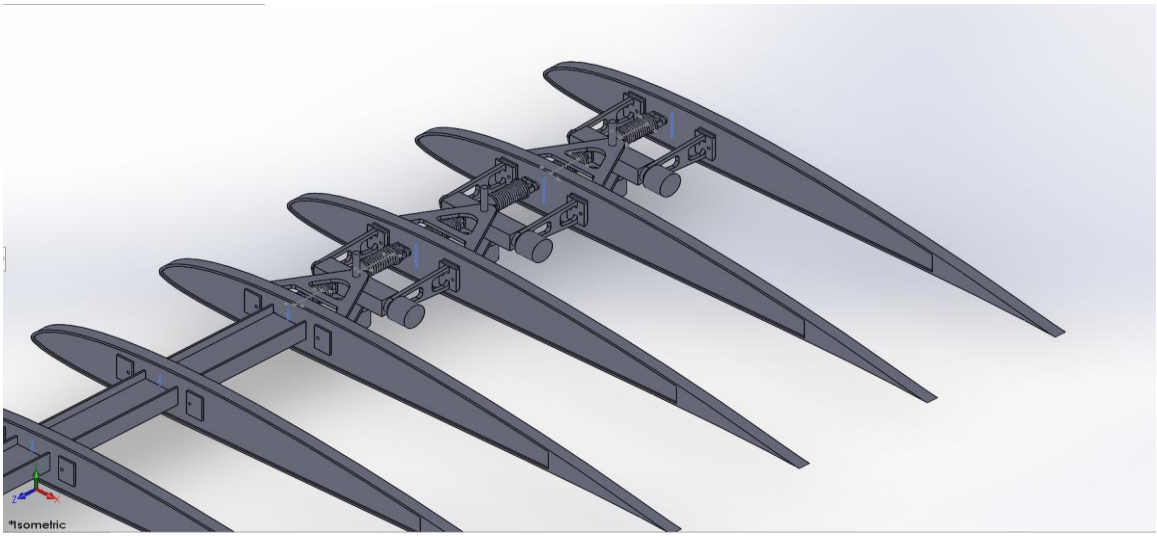

Fig. 3.25 Mechanism for spanwise adaptive wing

3.4 ANALYSIS OF THE WING

3.4.1 STRUCTURAL ANALYSIS & MATERIAL SELECTION FOR THE WING

Now analysis of the wing model is to be done which was designed in CAD software by importing it into ANSYS to perform static structural analyses with different materials and different cross sections for the spar. From literature survey it was found the mostly used cross-sections are C-section and I-sections for the wing spar. And the mostly used materials for the wing spar are Structural Steel, Aluminium 7075 T6, Aluminium 2024 T3 and for wing surface Epoxy Resin which is a composite material is fixed [15].

Fig. 3.26, 3.27 and 3.28 depicts the static structural analysis with Deformation for I-section and spar material as Structural Steel, Aluminium 7075 T6, Aluminium 2024 T3 respectively.

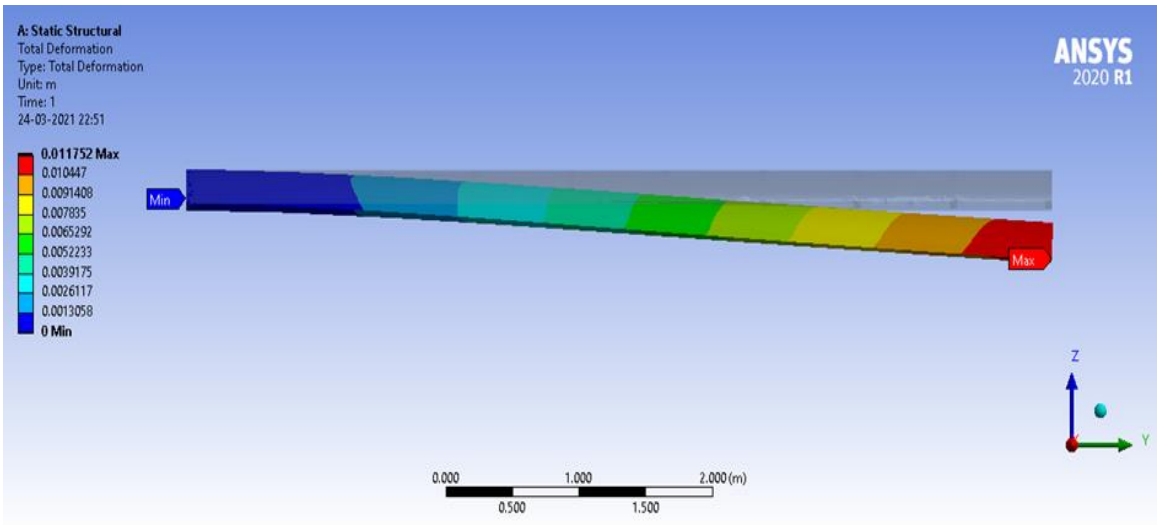

Fig. 3.26 Deformation for I-section & spar material as Structural Steel

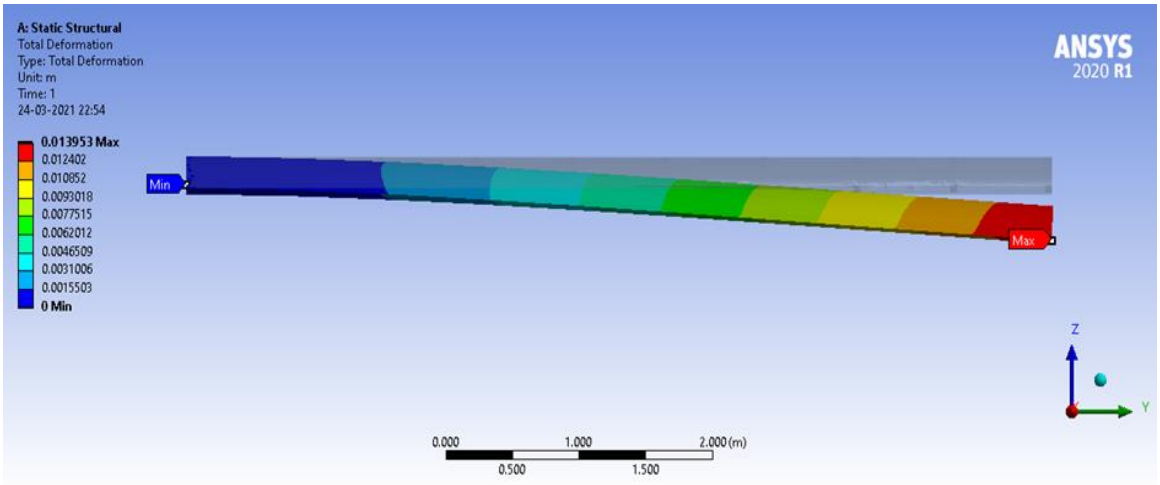

Fig. 3.27 Deformation for I-section & spar material as Aluminium 7075 T6

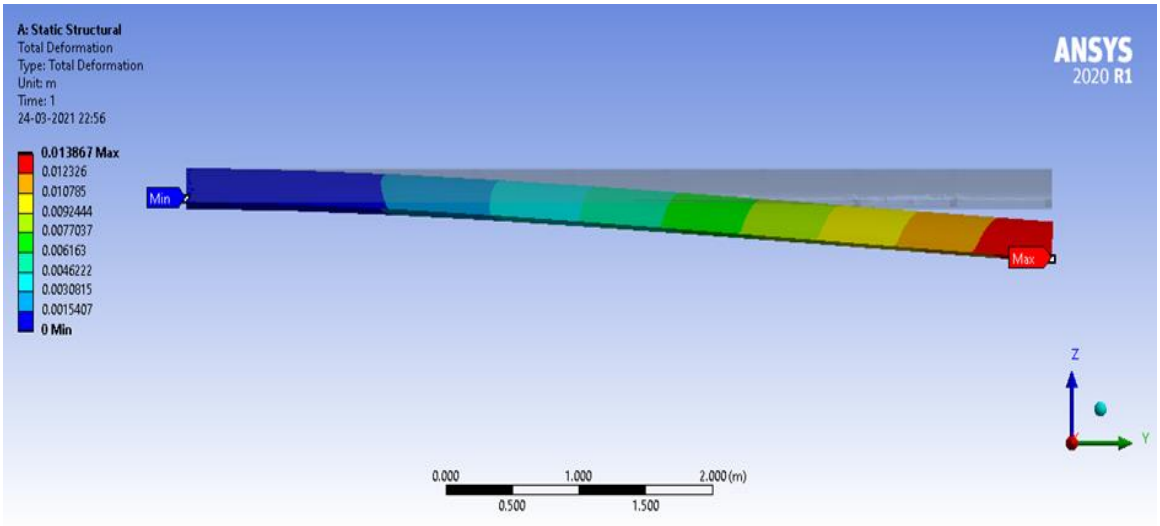

Fig. 3.28 Deformation for I-section & spar material as Aluminum 2024 T3

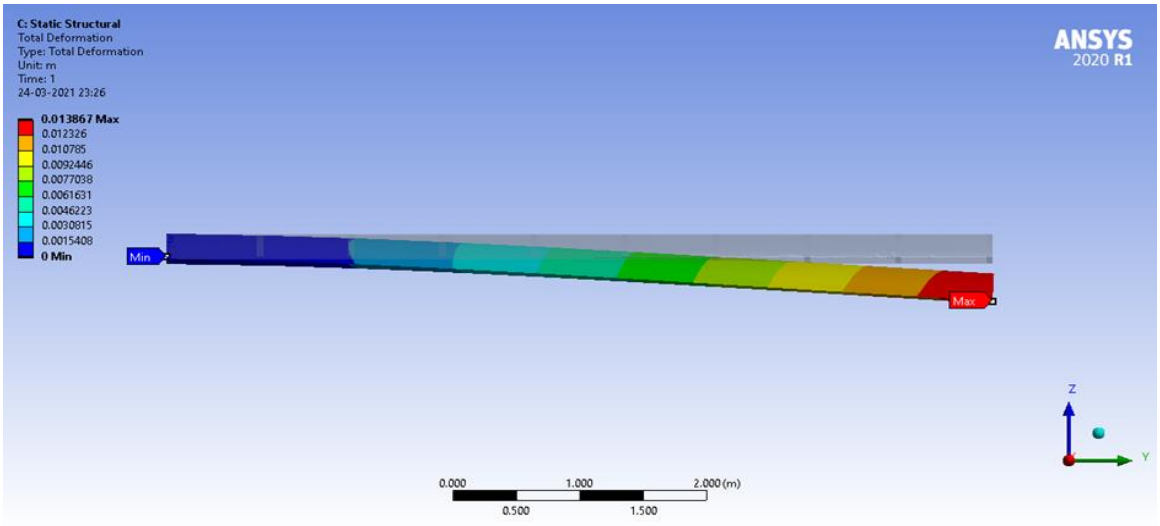

Fig. 3.29 Deformation for C-section & spar material as Structural Steel

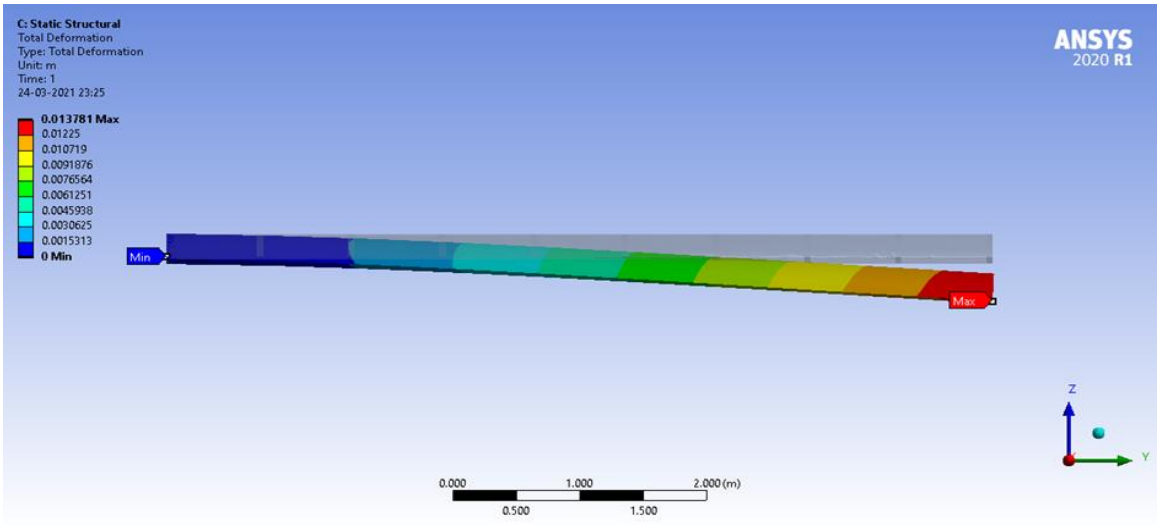

Fig. 3.30 Deformation for C-section & spar material as Aluminium 7075 T6

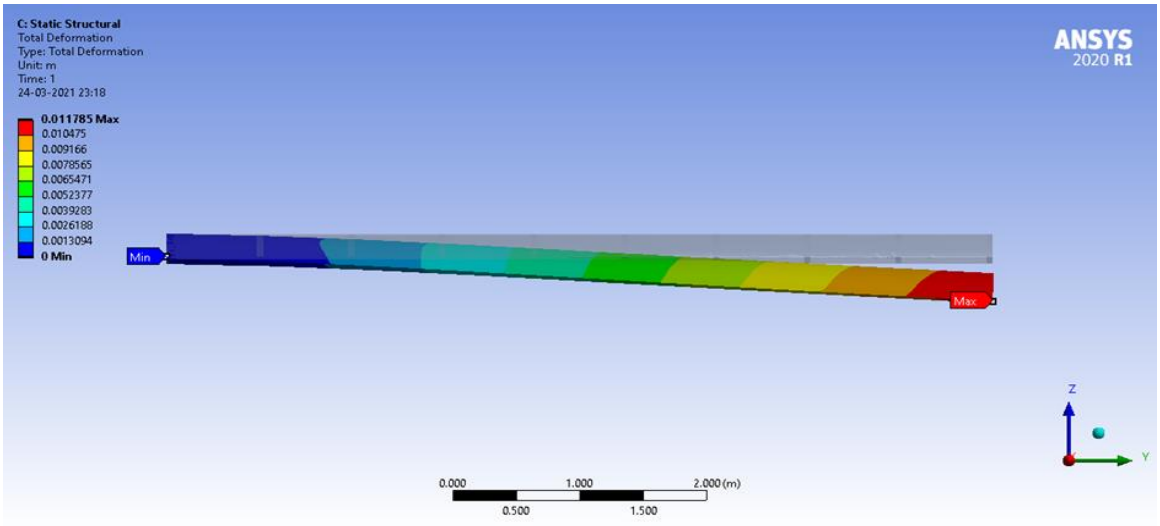

Fig. 3.31 Deformation for C-section & spar material as Aluminium 2024 T3

Fig. 3.29, 3.30 and 3.31 depicts the static structural analysis with Deformation for C-section and spar material as Structural Steel, Aluminium 7075 T6, Aluminium 2024 T3 respectively.

Fig. 3.32, 3.33 and 3.34 depicts the static structural analysis with Deformation due to self-weight and spar material as Structural Steel, Aluminium 7075 T6, Aluminium 2024 T3 respectively.

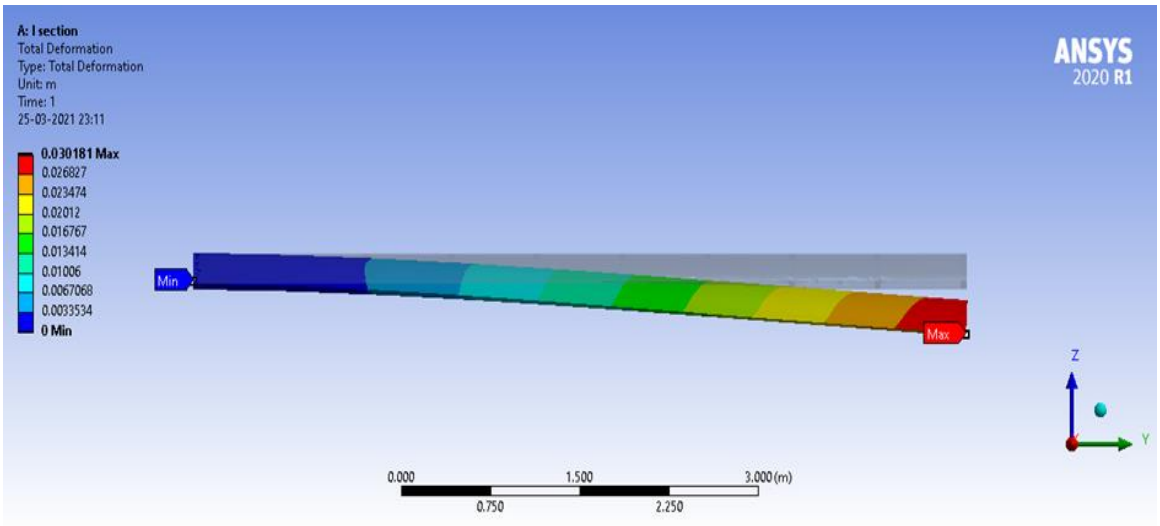

Fig. 3.32 Deformation due to self-weight & spar material as Structural Steel

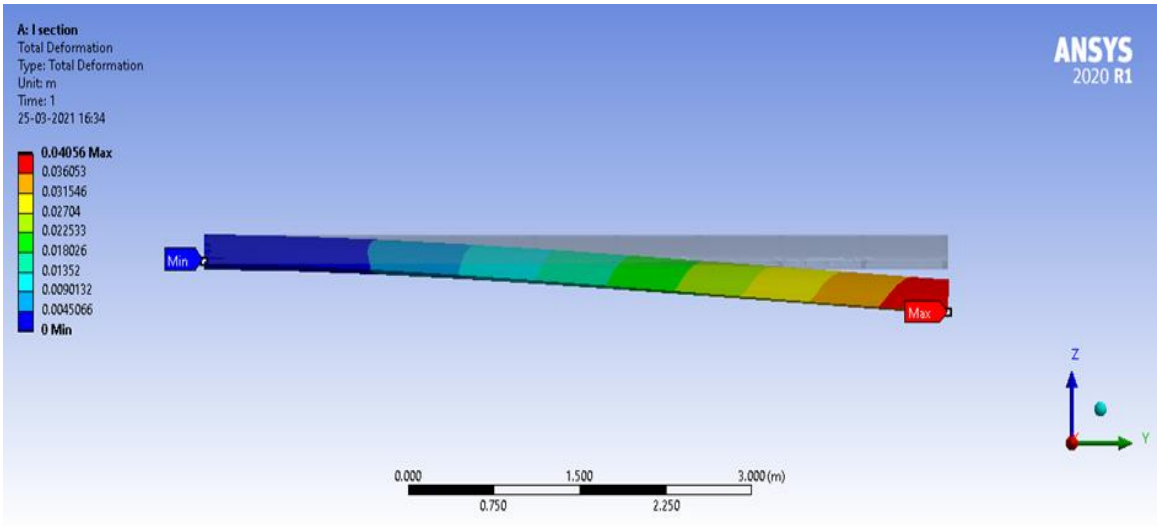

Fig. 3.33 Deformation for due to self-weight & spar material as Aluminium 7075 T6

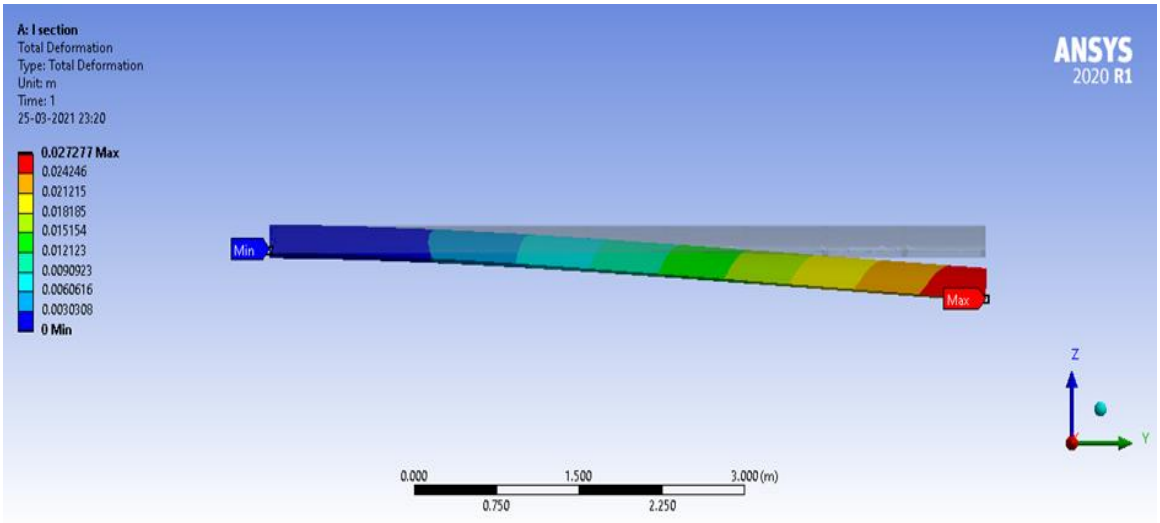

Fig. 3.34 Deformation due to self-weight & spar material as Aluminium 2024 T3

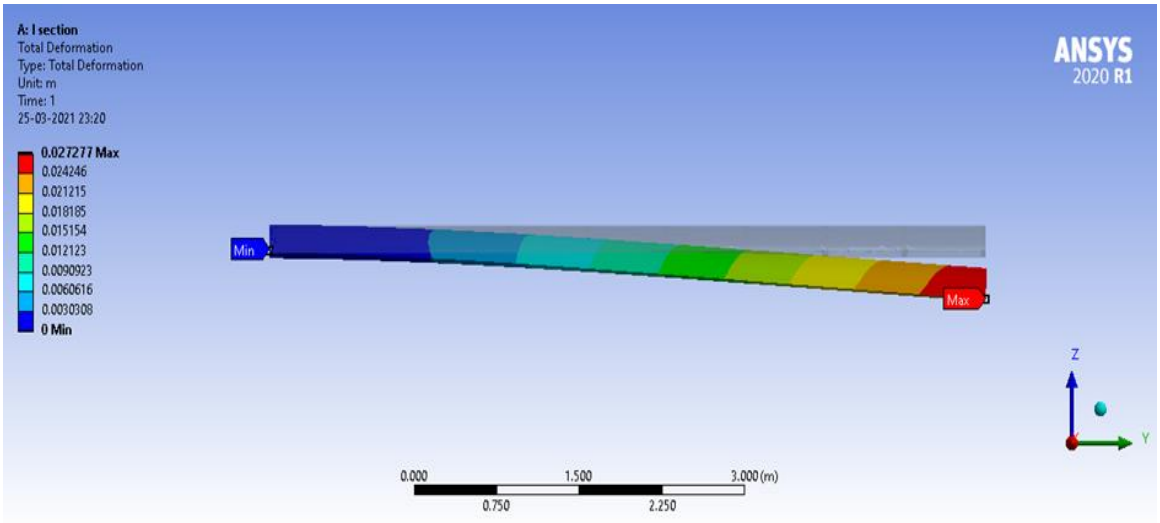

Fig. 3.35 Deformation due to ultimate load & spar material as structural Steel

Fig. 3.35, 3.36 and 3.37 depicts the static structural analysis with Deformation due to ultimate load with factor of safety as 1.5 [21] and spar material as Structural Steel, Aluminium 7075 T6, Aluminium 2024 T3 respectively.

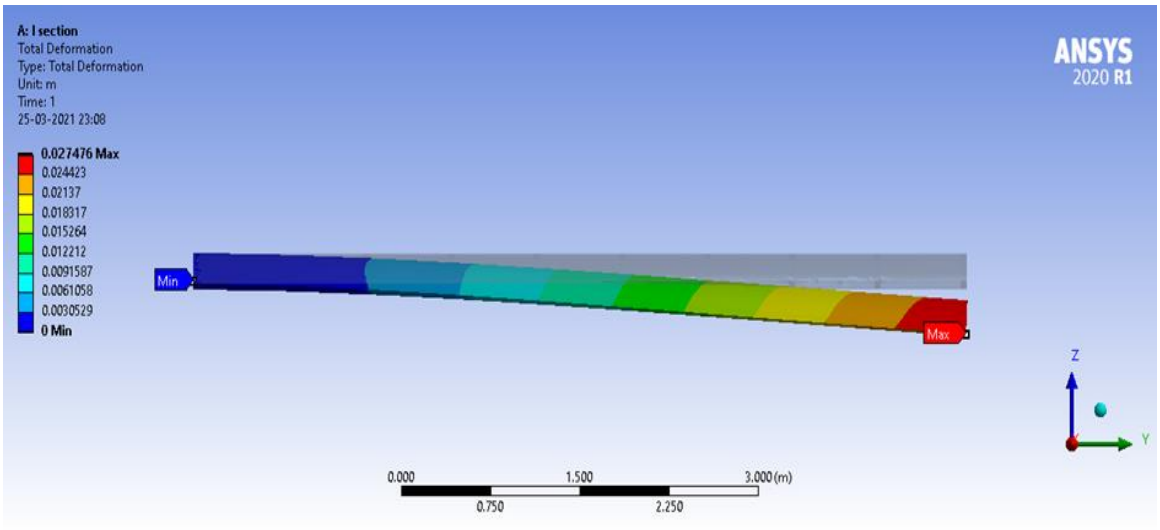

Fig. 3.36 Deformation due to ultimate load & spar material as Aluminium 7075 T6

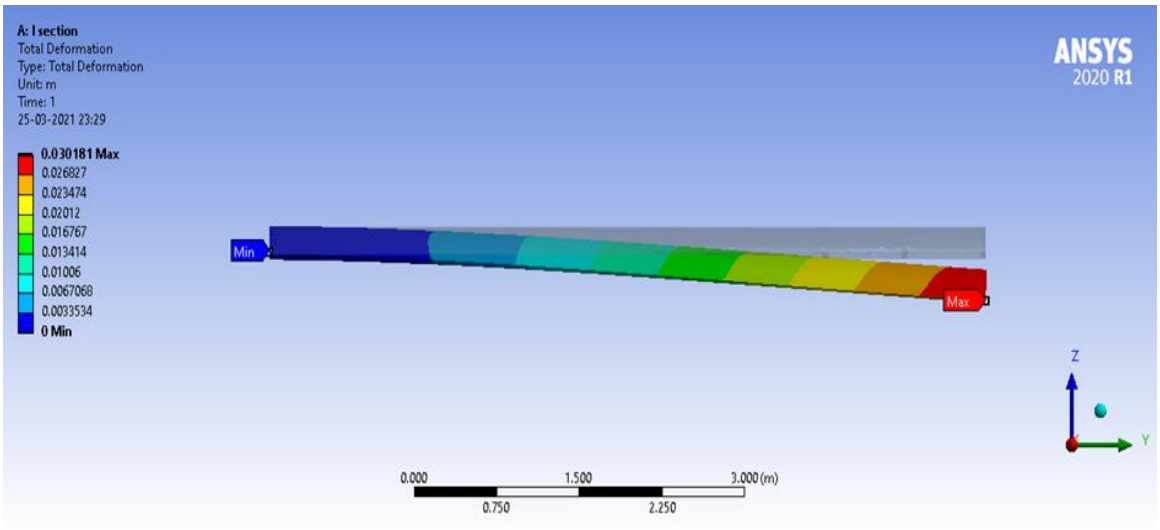

Fig. 3.37 Deformation due to ultimate load & spar material as Aluminium 2024 T3

Based on analysis performed for cross section of spar and material selection the various results have been tabulated and discussed in Chapter 4.

3.4.2 WING MODAL ANALYSIS

Modal analysis is performed to provide the vibrational property of wing structure. Fig. 3.38 depicts the deformation for 1st ,2nd ,3rd ,4th and 5th mode respectively.

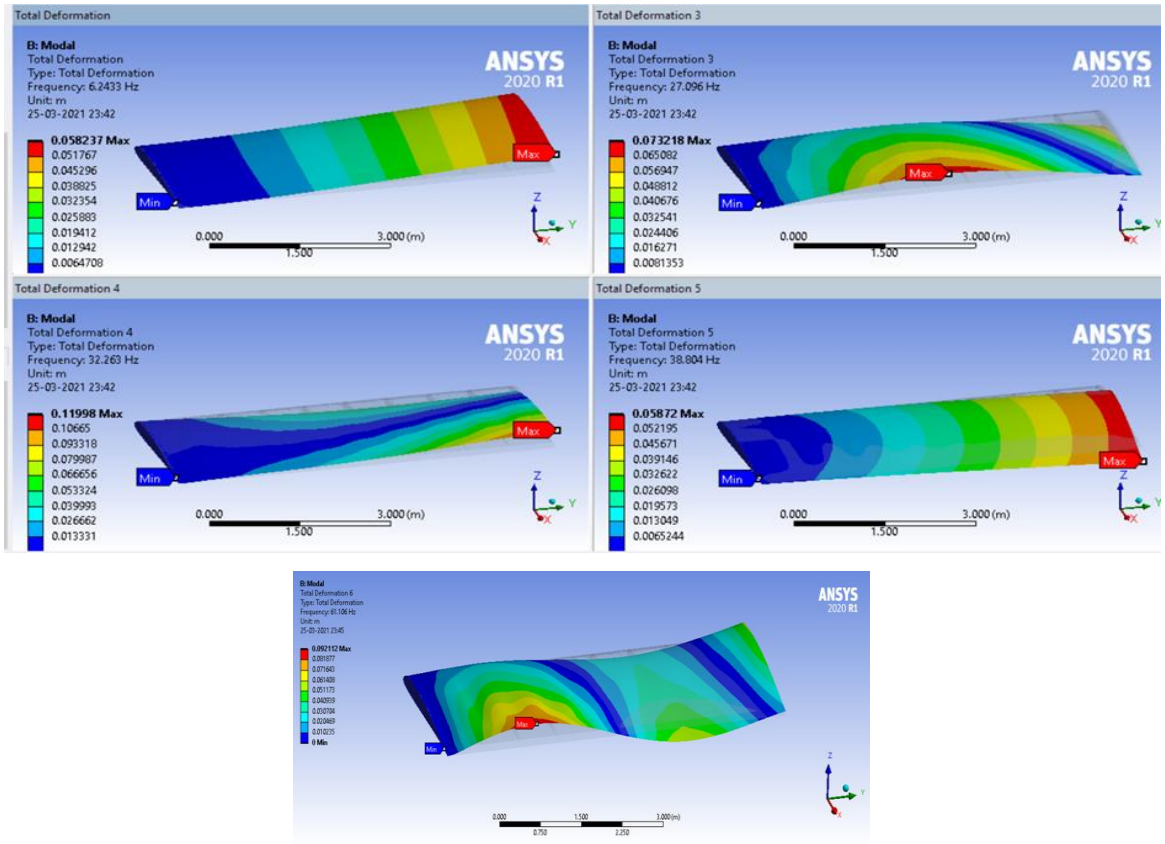

Fig. 3.38 Total deformation for 5 subsequent modes of the wing

3.4.3 CFD ANALYSIS OVER THE WING

The wing model needs to be analyzed for the comparison between the spanwise, sweep, and plain wing. The wing has to be analyzed in 150, 200 and 250 m/s. These velocities have been chosen since the problem statement mentions for higher subsonic range and to help the wing to move with less power by decreasing drag. The meshing is performed and flow has been analyzed with pressure distribution and velocity distribution has been observed and various lift and drag values have been observed and tabulated.

3.4.3.1 CFD ANALYSIS OF SPANWISE ADAPTIVE WING

Properties used for analysing the spanwise adaptive wing

- Wing is given structured mesh.
- Wing is bent by 60° downwards.
- Face meshing is given to all the faces and edge sizing is given as per the requirements. Meshing on the bent faces is focused.
- Domain is nearly 5 times the size of the model.
- The domain has been given structured mesh.

Fig. 3.39 represent the meshing of spanwise adaptive wing. Fig. 3.40 represents the pressure distribution over the spanwise adaptive wing and Fig. 3.41 represents the velocity distribution over the spanwise adaptive wing.

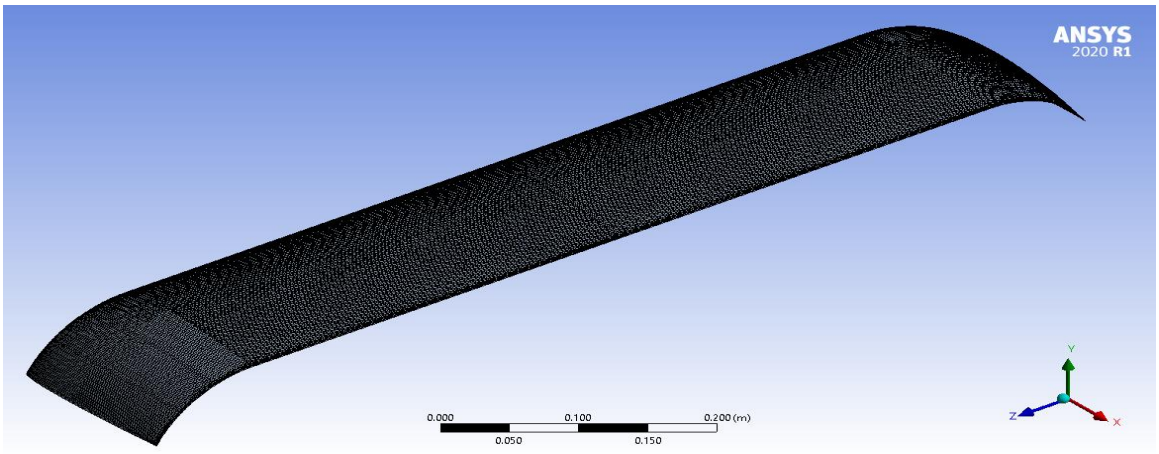

Fig. 3.39 Meshing of spanwise adaptive wing

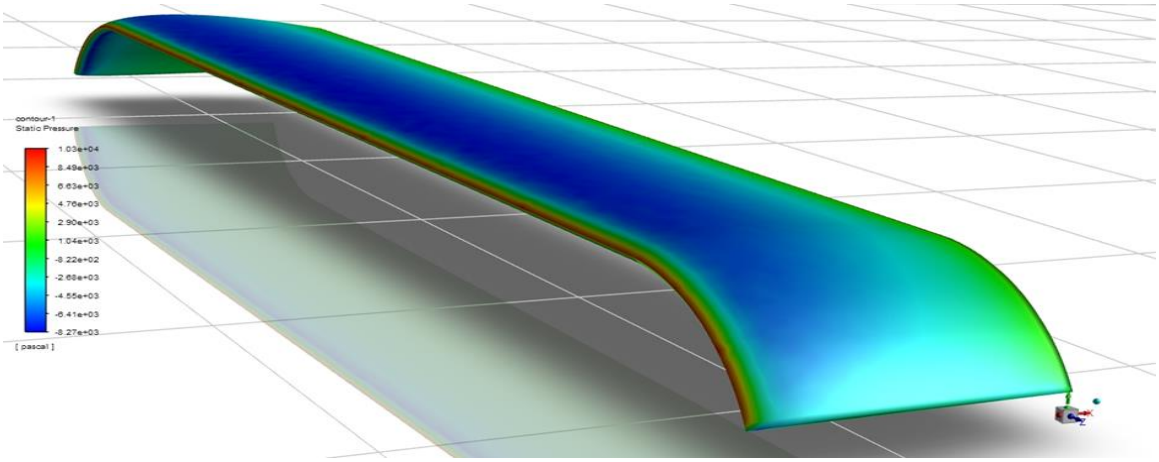

Fig. 3.40 Pressure distribution over the spanwise adaptive wing

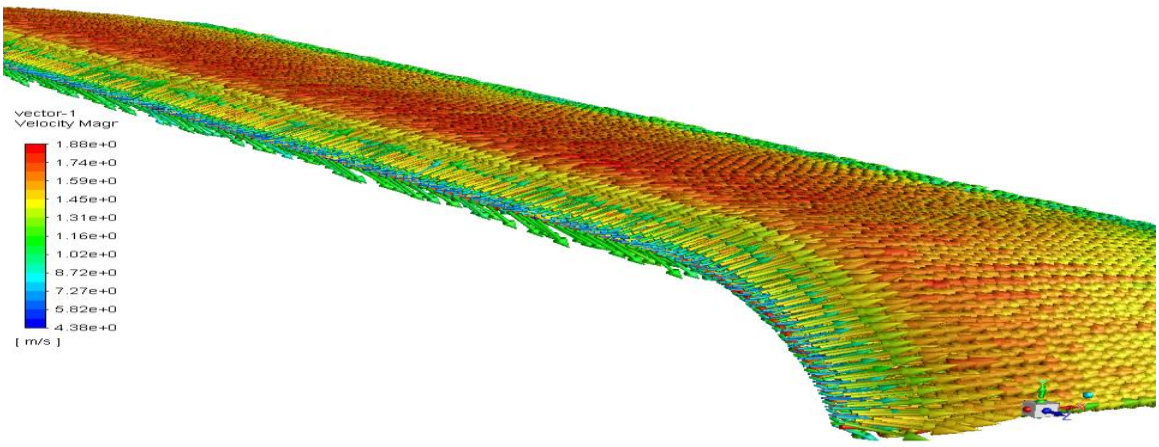

Fig. 3.41 Velocity distribution over the spanwise adaptive wing

3.4.3.2 CFD ANALYSIS OF SWEEP/SWEPT WING

Properties used for analysing the sweep wing

- Wing is given structured mesh.
- Wing is swept back by 50°.
- Face meshing is given to all the faces and edge sizing is given as per the requirements. Leading edge and trailing edge sizing are different to create proper mesh. Meshing on the bent faces is focused.
- Domain is nearly 5 times the size of the model.
- The domain has been given structured mesh.

Fig. 3.42 represent the meshing of sweep wing; Fig. 3.43 represents the pressure distribution over the sweep wing.

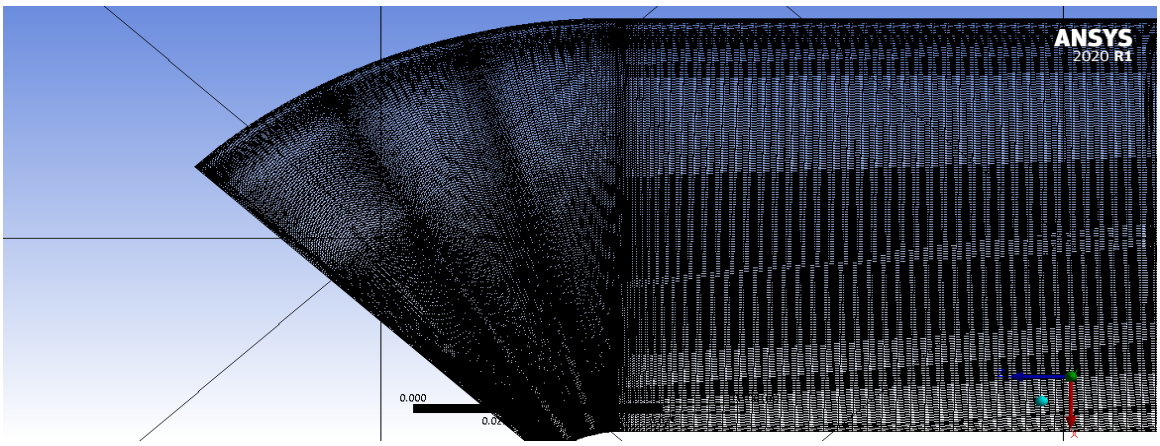

Fig. 3.42 Meshing of swept wing

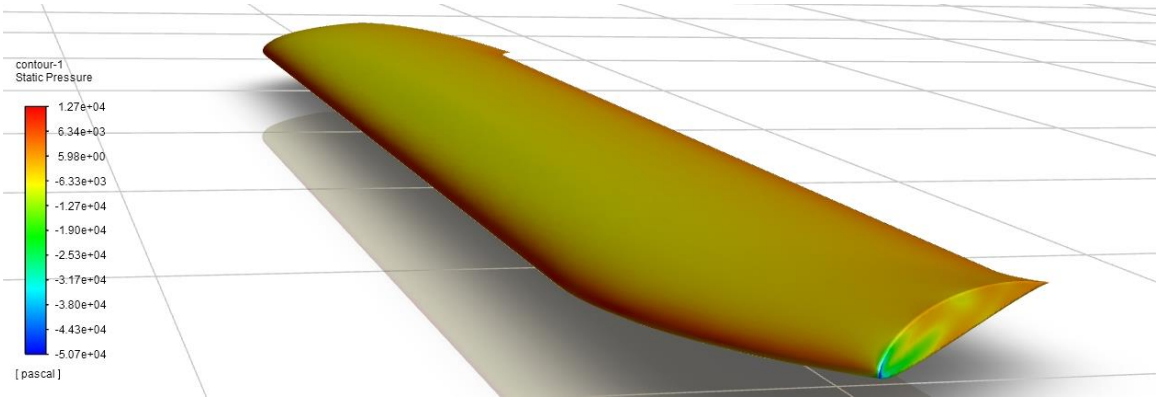

Fig. 3.43 Pressure distribution over the swept wing

3.4.3.3 CFD ANALYSIS OF PLAIN WING

Properties used for analysing the plain wing

- Wing is given structured mesh.

- Face meshing is given to all the faces and edge sizing is given as per the requirements.
- Domain is nearly 5 times the size of the model.

Fig. 3.44 represents the pressure distribution over the flat wing.

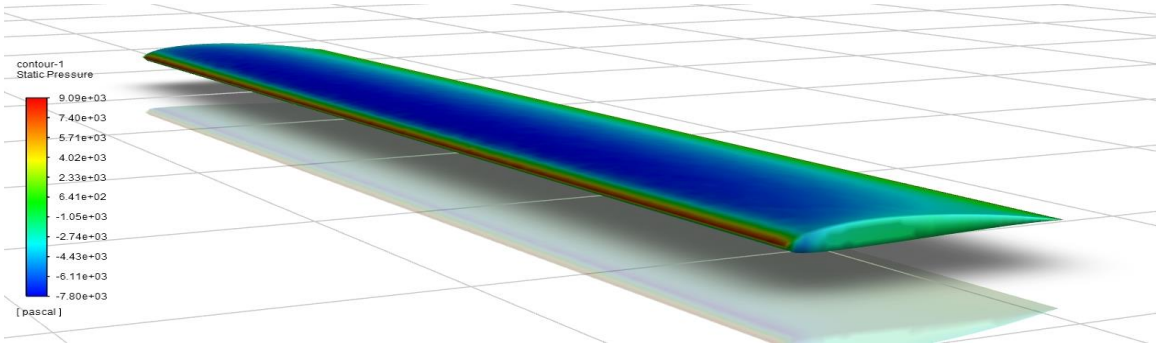

Fig. 3.44 Pressure distribution over the flat wing

CHAPTER 4

RESULTS AND DISCUSSIONS

4.1 CFD ANALYSIS ON AIRFOILS

4.1.1 ANALYTICAL RESULTS OF AIRFOIL

Plotting the graphs at various angles of attack and finding lift, drag, and the ratio of lift to drag for each airfoil and at different velocities that is 15m/s, 35m/s, and 55m/s.

Fig. 4.1 depicts the lift, drag, and L/D ratio at a velocity of 15m/s for Clark-Y airfoil which interprets that lift is increasing and then experiencing stalls near to 10°.

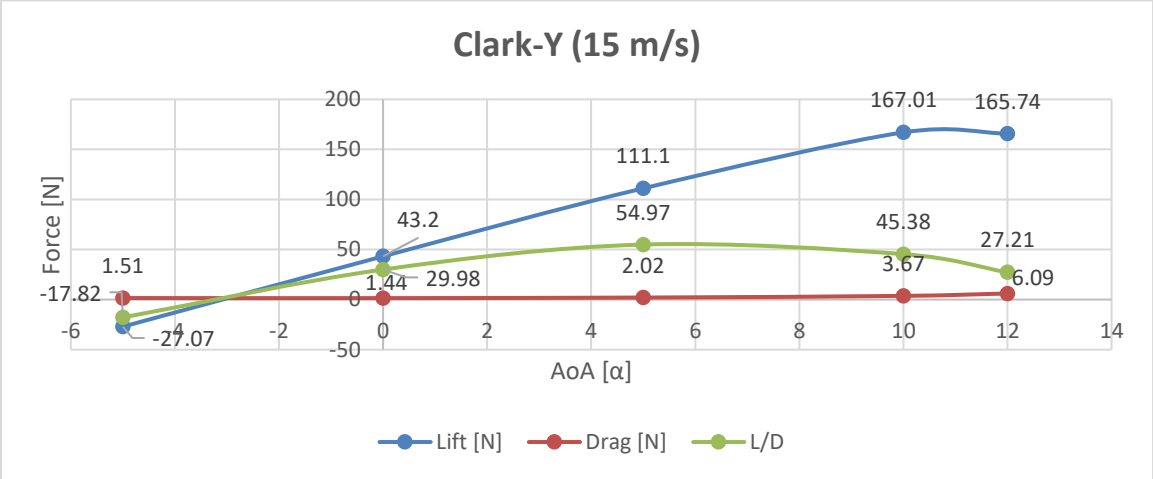

Fig. 4.1 Plot of Lift, Drag, and L/D ratio of Clark-Y airfoil at various AoA at 15m/s

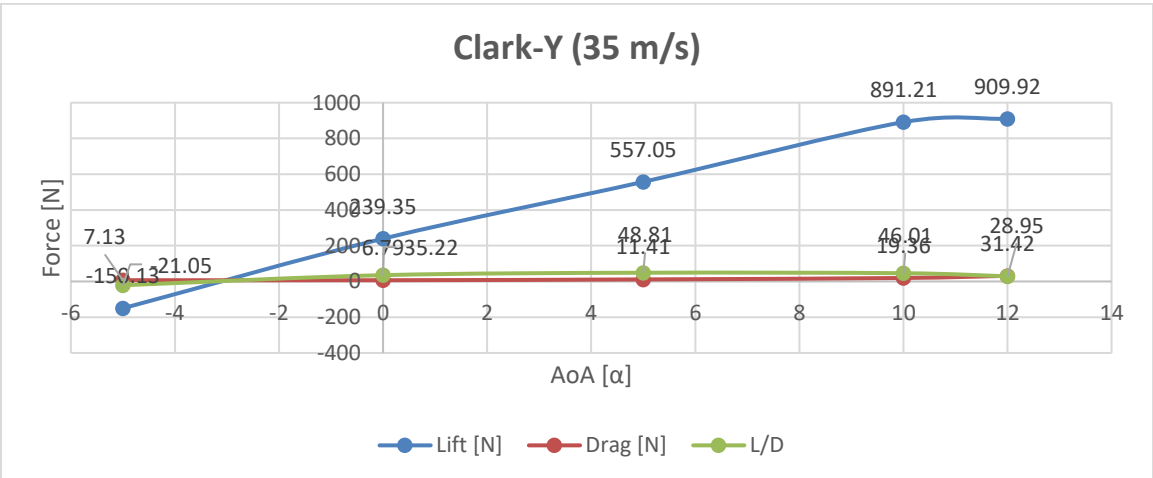

Fig. 4.2 Plot of Lift, Drag, and L/D ratio of Clark-Y airfoil at various AoA at 35m/s

Fig. 4.2 depicts the lift, drag, and L/D ratio at a velocity of 35m/s for Clark-Y airfoil which interprets that lift is increasing and then experiencing stalls near to 10.5°. Fig. 4.3 depicts the lift, drag, and L/D ratio at a velocity of 55m/s for Clark-Y airfoil which interprets that lift is increasing and then experiencing stalls near to 12°.

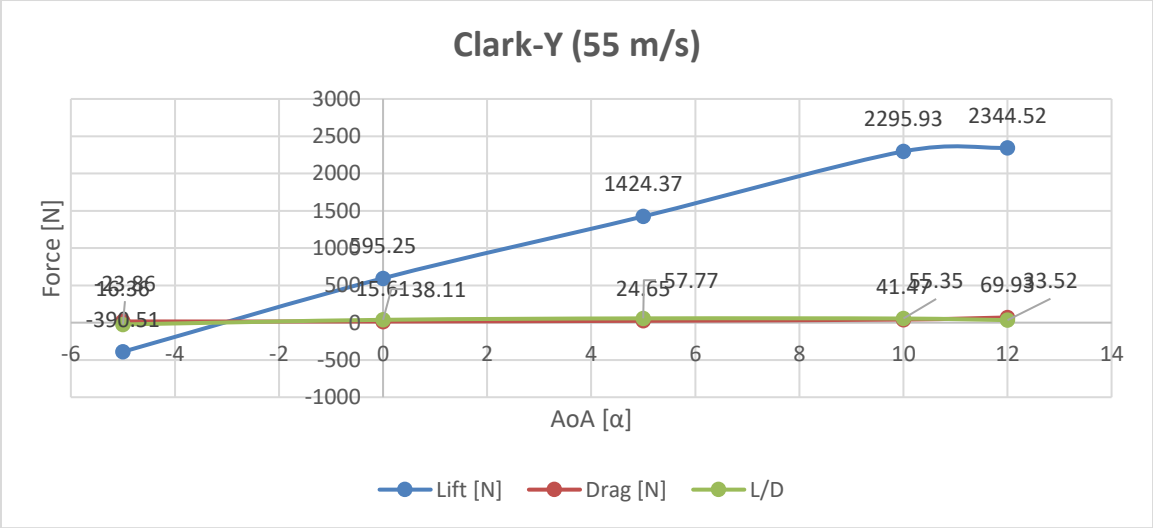

Fig. 4.3 Plot of Lift, Drag, and L/D ratio of Clark-Y airfoil at various AoA at 55m/s

Fig. 4.4 depicts the lift, drag, and L/D ratio at a velocity of 15m/s for E387 airfoil which interprets that lift is increasing and then experiencing stall near to 10°.

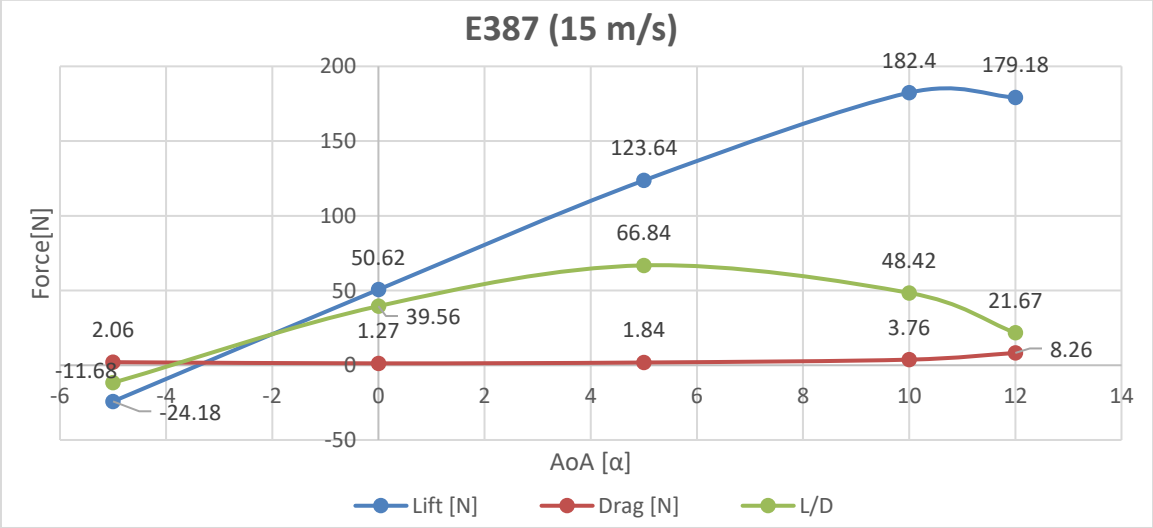

Fig. 4.4 Plot of Lift, Drag, and L/D ratio of E387 airfoil at various AoA at 15m/s

Fig. 4.5 depicts the lift, drag, and L/D ratio at a velocity of 35m/s for E387 airfoil which interprets that lift is increasing and then experiencing stall between a range of 10°-10.5°. Fig. 4.6 depicts the lift, drag, and L/D ratio at a velocity of 55m/s for E387 airfoil which interprets that lift is increasing and then experiencing stall at 11°.

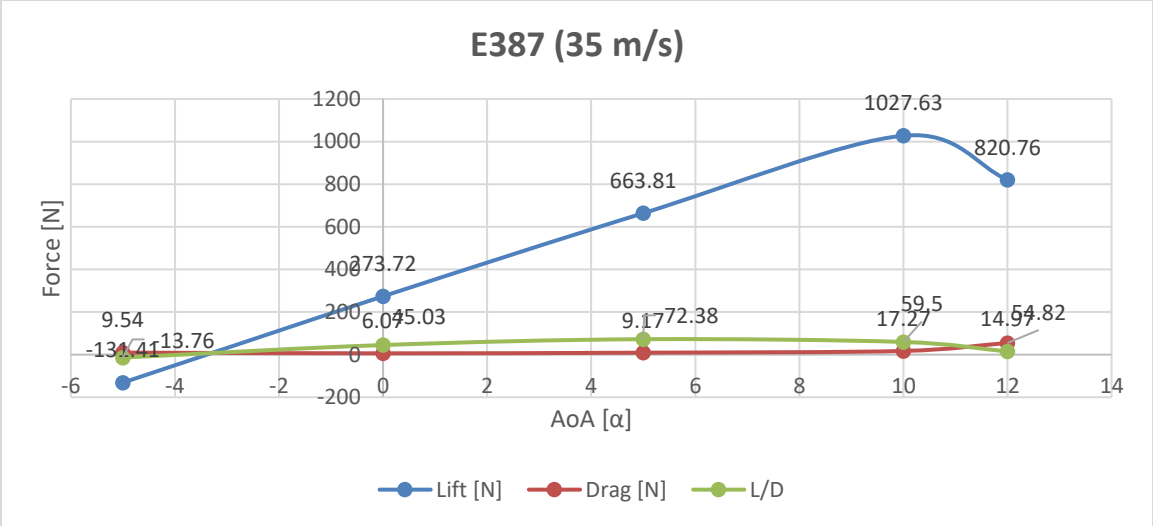

Fig. 4.5 Plot of Lift, Drag, and L/D ratio of E387airfoil at various AoA at 35m/s

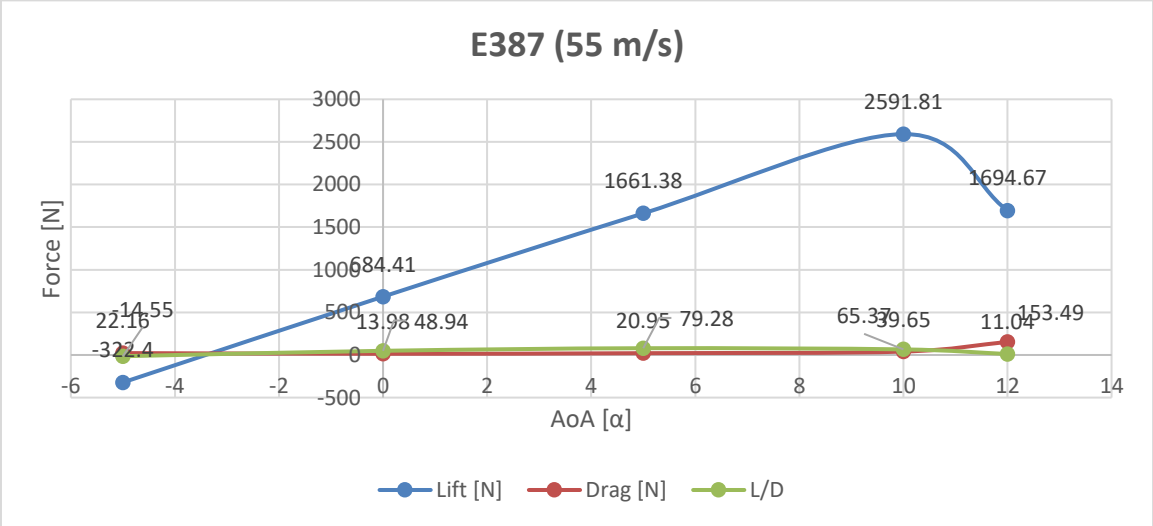

Fig. 4.6 Plot of Lift, Drag, and L/D ratio of E387 airfoil at various AoA at 55m/s

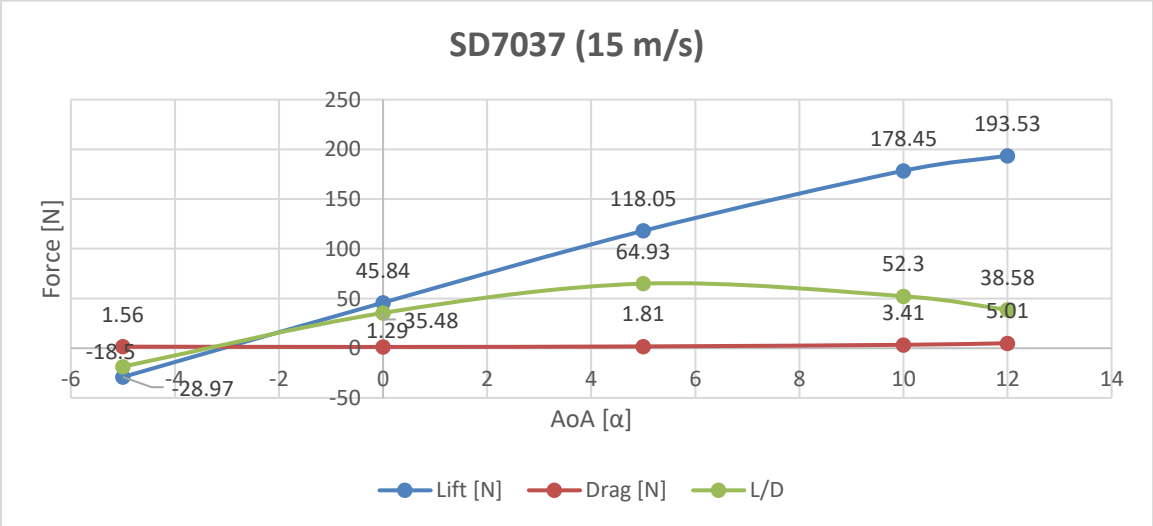

Fig. 4.7 Plot of Lift, Drag, and L/D ratio of SD7037 airfoil at various AoA at 15m/s

Fig. 4.7 depicts the lift, drag, and L/D ratio at a velocity of 15m/s for SD7037 airfoil which interprets that lift is increasing and then experiencing stall between a range of 14°-16°. Fig. 4.8 depicts the lift, drag, and L/D ratio at a velocity of 35m/s for SD7037 airfoil which interprets that lift is increasing and then experiencing stall between a range of 12°-13°.

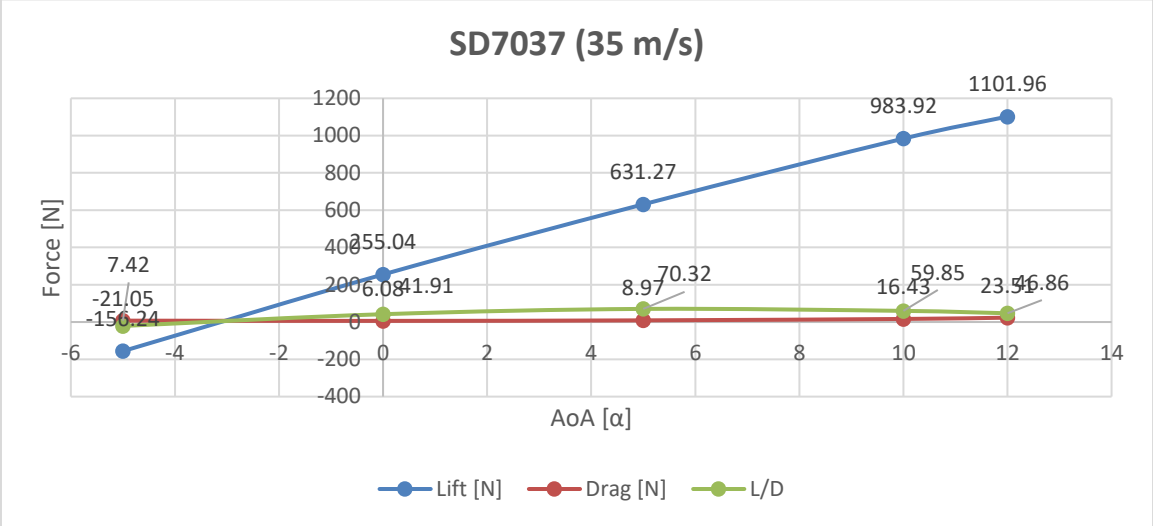

Fig. 4.8 Plot of Lift, Drag, and L/D ratio of SD7037 airfoil at various AoA at 35m/s

Fig. 4.9 depicts the lift, drag, and L/D ratio at a velocity of 55m/s for SD7037 airfoil which interprets that lift is increasing and then experiencing stall between a range of 12°-13°. Table 4.1, 4.2 and 4.3 depicts the values of lift, drag and its co-efficient for the airfoil E387, Clark-Y and SD7037 respectively.

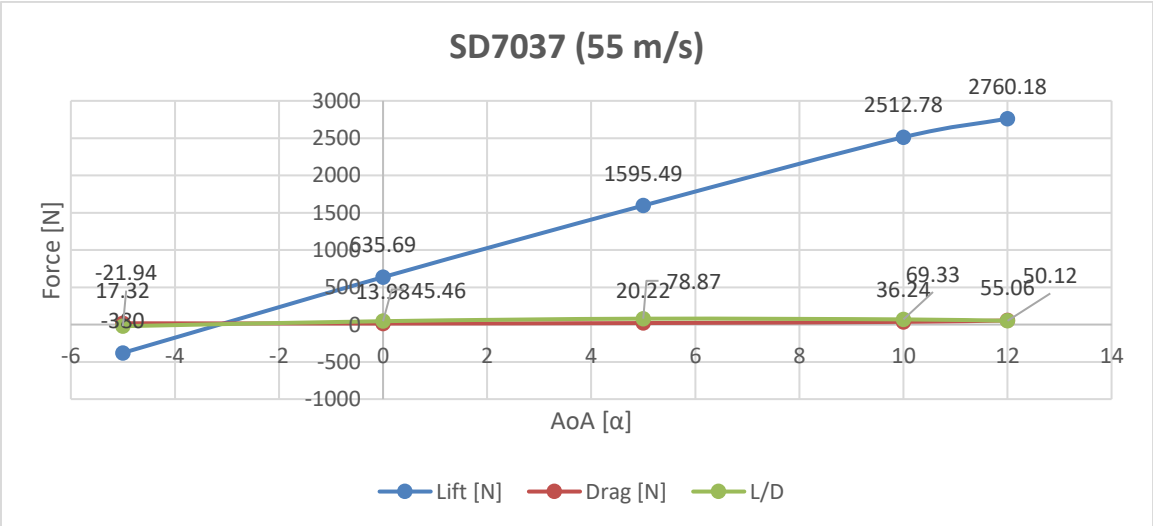

Fig. 4.9 Plot of Lift, Drag, and L/D ratio of SD7037 airfoil at various AoA at 55m/s

Table 4.1 Various aerodynamic characteristics at different AoA for E387 airfoil

α (in Degrees)	Inlet Velocity [m/s]	Lift [N]	Drag [N]	C_L	C_D	C_L/C_D
-5	15	-24.188	2.06958	-0.175514	0.015017	-11.6874
0	15	179.18	8.2685	1.3001723	0.059998	21.67019
5	15	50.6249	1.27966	0.3673462	0.009286	39.56121
10	15	123.645	1.84982	0.8971972	0.013423	66.84164
12	15	182.407	3.76671	1.3235882	0.027332	48.42608

Table 4.2 Various aerodynamic characteristics at different AoA for Clark-Y airfoil

α (in Degrees)	Inlet Velocity [m/s]	Lift [N]	Drag [N]	C_L	C_D	C_L/C_D
-5	15	-27.076	1.51883	-0.19647	0.011021	-17.8273
0	15	43.2007	1.44051	0.313474	0.010453	29.98986
5	15	111.103	2.02083	0.80619	0.014664	54.97889
10	15	167.015	3.67968	1.2119	0.026701	45.38846
12	15	165.749	6.09118	1.202714	0.044199	27.21131

Table 4.3 Various aerodynamic characteristics at different AoA for SD7037 airfoil

α (in Degrees)	Inlet Velocity [m/s]	Lift [N]	Drag [N]	C_L	C_D	C_L/C_D
-5	15	-28.975	1.56543	-0.21025	0.011359	-18.5095
0	15	45.8495	1.29193	0.332695	0.009375	35.48915
5	15	118.058	1.81796	0.856657	0.013192	64.93982
10	15	178.453	3.41207	1.294897	0.024759	52.30051
12	15	193.532	5.01592	1.404314	0.036397	38.58355

Our application is towards higher subsonic speeds so it is important to see the plot of drag versus Mach number. As Mach no. increases it reaches a point of critical Mach number. Critical Mach no. is a point where the Mach no. in front of the airfoil is less than sonic Mach no. but the Mach no. on the airfoil has a point where flow creates shocks and increases drag to large values due to which airfoil fails at those speeds.

How does the flow reach unit Mach number on airfoil?

Airfoils gains lift by velocity in above half of airfoil is increased hence creating a low pressure and below half of an airfoil velocity is decreased and pressure is reduced. This

change in pressure creates lift. And because of this high velocity approach the local Mach no. on above half of an airfoil reaches unity and enters supersonic speeds which creates shocks and hence increasing drag.

Fig. 4.10 depicts how drag increases as the plot moves to higher speeds of 150m/s, 200m/s and 250m/s due to effect of critical Mach no. and drag divergence Mach no. at different angle of attack for Clark-Y airfoil.

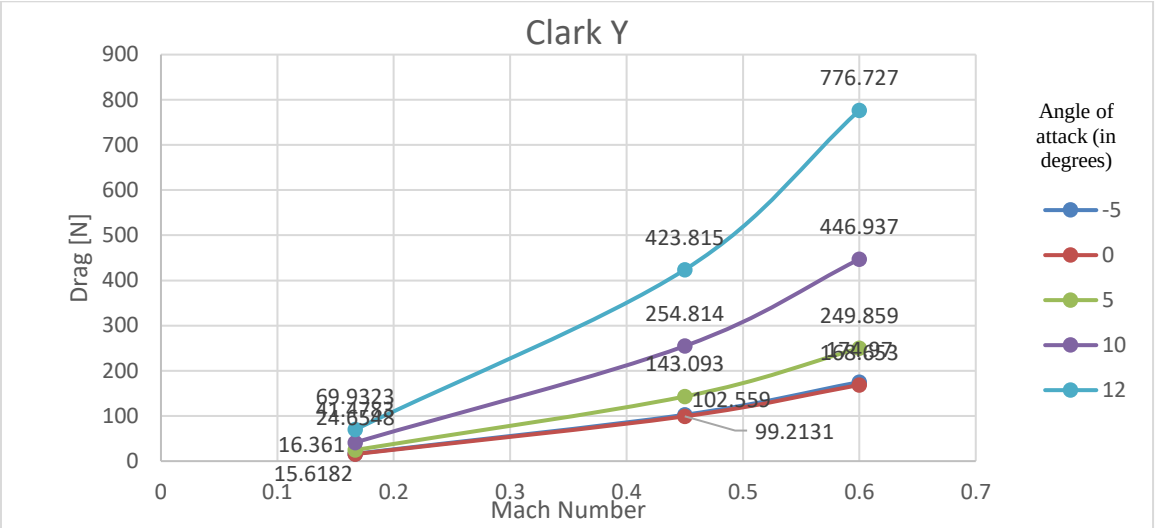

Fig. 4.10 Plot of Drag vs Mach no. for Clark-Y airfoil

Fig. 4.11 depicts how drag increases as the plot moves to higher speeds of 150m/s, 200m/s and 250m/s due to effect of critical Mach no. and drag divergence Mach no. at different angle of attack for E387 airfoil.

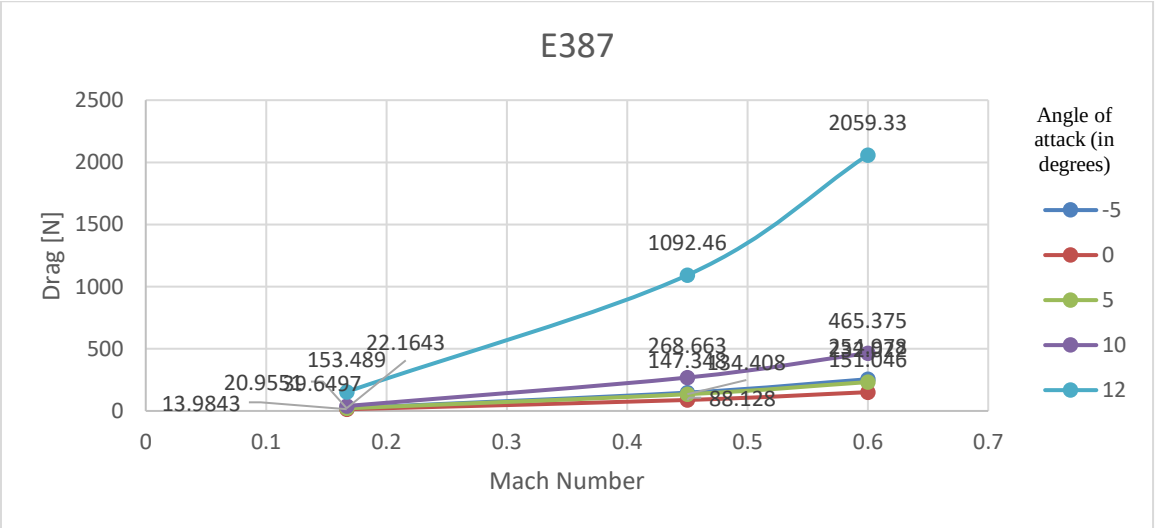

Fig. 4.11 Plot of Drag vs Mach no. for E387 airfoil

Fig. 4.12 depicts how drag increases as the plot moves to higher speeds of 150m/s, 200m/s and 250m/s due to effect of critical Mach no. and drag divergence Mach no. at different angle of attack for SD7037 airfoil.

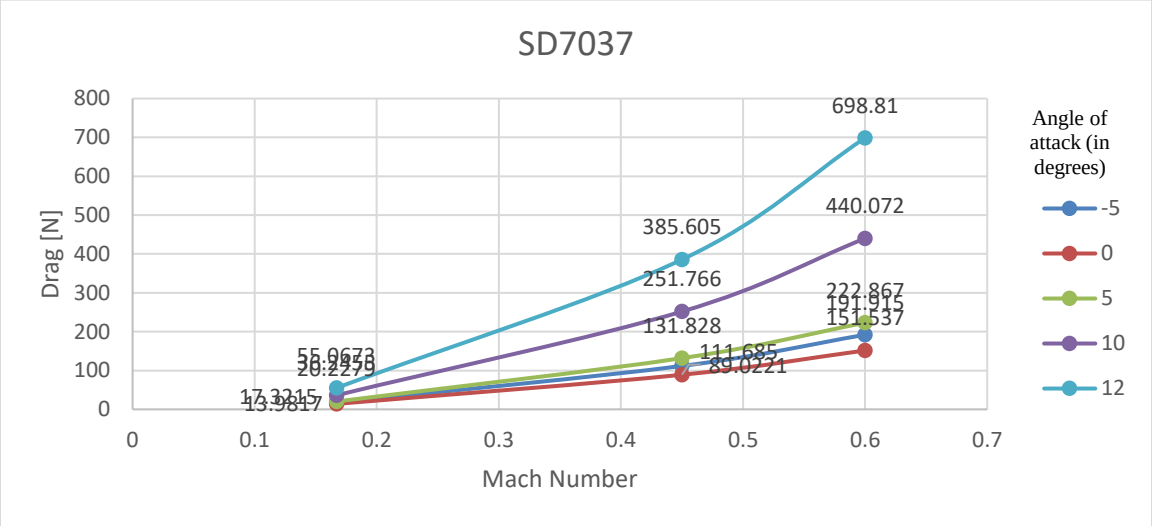

Fig. 4.12 Plot of Drag vs Mach no. for SD7037 airfoil

4.1.2 DISCUSSION ON AIRFOILS BASED ON RESULTS

The lift, drag, and their co-efficient values for a different angle of attacks have been tabulated for all the three airfoils i.e., E387, Clark-Y, and SD7037.

There was a very minute difference in the properties of Clark-Y, E387 and SD7037 with the following characteristics of high lift less drag and high lift to drag ratio as seen. But due to the application of higher subsonic ranges the drag versus Mach no. plot has to be observed to check if the drag is not increasing to a very high value and creating stall at lower speeds.

The best airfoil is to be selected based on the criteria's below:

1. The airfoil which has the highest maximum lift coefficient.
2. The airfoil which has the lowest minimum drag coefficient.
3. The airfoil which has the highest lift-to-drag ratio.
4. The airfoil which has the highest lift curve slope.

Based on these conditions the discussion on the 3 airfoils is made below:

- The E387 airfoil has the best L/D ratio and good lift values at various velocities but the drawback is that the stalling angle is small and it is steep downwards as it reaches the stall angle. Because of that E387 has been rejected.
- The Clark-Y airfoil has a good L/D ratio and good lift values and low drag values at various velocities and also stalling angle greater than 12 degrees. But at higher

speeds, the lift values become less, and drag increases compared to the other airfoil. Hence Clark-Y airfoil has been rejected.

- The SD7037 airfoil has the best lift values, low drag values, and greater stalling angle. Along with this, it has the best performance even at a greater speed which is matching with our application, which is using it at higher speeds. By observing the graphs, it is clearly seen that SD7037 has less drag at higher speeds and even at high angle of attacks the drag value is less compared to another airfoil.

Hence, we finalize the airfoil SD7037 for modelling of the wing.

4.2 WING ANALYSIS DISCUSSION

4.2.1 WING STRUCTURAL ANALYSIS AND MATERIAL SELECTION

All the results done using structural analysis in ANSYS are tabulated below in Table 4.4 and it depicts the deformations observed for 2 cross-sections I and C shaped spars. Based on the values obtained use of I-section has been finalized for further development of wing.

Table 4.4 Deformations based on analyses

Material	I – Section (mm)	C – Section (mm)
Structural Steel	13.953	13.867
Aluminium 7075 T6	11.752	11.785
Aluminium 2024 T3	13.867	13.781

Structural analysis for self-weight and ultimate load acting on it for different materials is performed and based on values obtained it has been observed that Aluminum 7075 T6 is best material among the materials on which structural analysis was performed. Table 4.5 depicts the values obtained while analyzing structurally due to self-load and ultimate load by keeping factor of safety as 1.5.

Table 4.5 Deformation due to self-weight and ultimate load

Material	Deformation due to self-weight(mm)	Deformation due to Ultimate load (mm)
Structural Steel	30.181	40.56
Aluminium 7075 T6	27.277	29.959
Aluminium 2024 T3	27.476	30.181

4.2.2 WING MODEL ANALYSIS

Modal analysis is performed for subsequent modes and the various frequencies have been tabulated below as in Table 4.6. This is performed for going through the vibrational properties at different modes and getting the natural frequencies or the frequencies at which wing might fail.

Table 4.6 Modal Analysis Frequencies at various modes

Mode	Frequencies (Hz)
1	6.264118445840
2	27.17027033157
3	32.33938533839
4	38.92384988216
5	61.26491538880

4.2.3 INDEPENDENT GRID ANALYSIS FOR CFD

Grid convergence is the name used to illustrate the improvement of results by using successive finer grids for the calculations. A calculation should move nearer to the correct answer as the mesh turn into finer, therefore the name grid convergence. Grid dependency study is an essential part of the computational exercise by which discretization error can be minimized to get consistent and stable values. A grid dependency study was done to ensure that the solution does not depend upon the grid quality and the grid size. As the difference between medium and fine grids it is observed that very less variation is found in analysis results so for less computation time for analysis medium grid for meshing is used to perform analysis. Fig. 4.13 depicts the plot of lift force versus the number nodes.

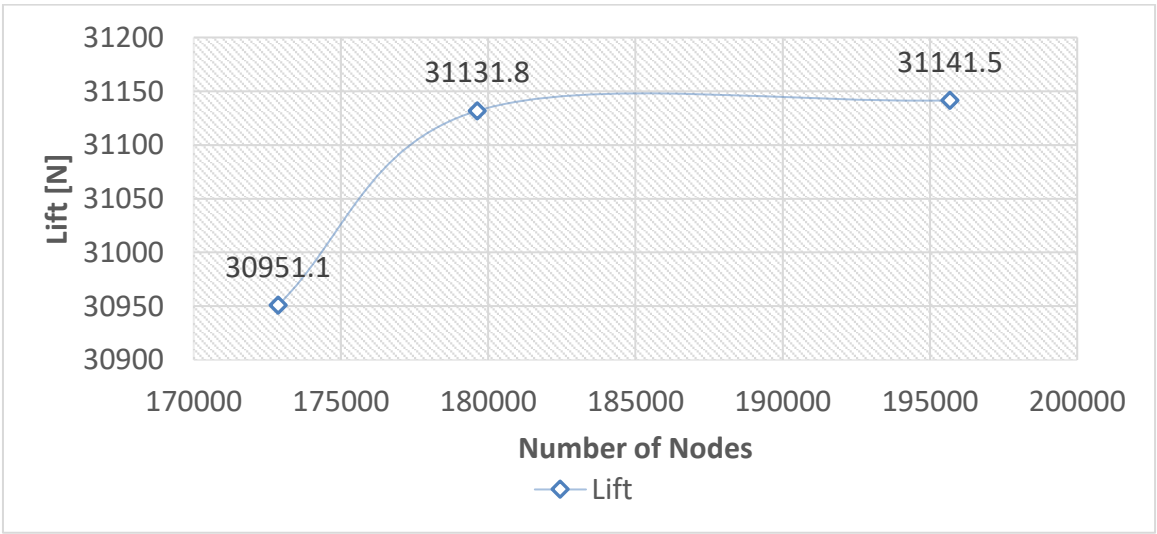

Fig. 4.13 Grid independent analyses for the wing

4.2.4 WING FLOW ANALYSIS

Now the final model of the wing with ribs, spar and the skin of the wing is to be analyzed. Then performing analysis over a velocity of 150 m/s, 200m/s and 250m/s which is a standard (based on our problem statement), fixed for this aircraft wing to perform any type of CFD analysis. Table 4.7, 4.8 and 4.9 depicts the results obtained during flow analysis at 150, 200 and 250 m/s for spanwise adaptive wing, swept wing and plain wing respectively.

Table 4.7 Results of Flow Analysis for Spanwise Wing

	Velocity [m/s]	Lift [N]	Drag [N]	L/D
1.	150	452.08	30.56	14.79
2.	200	805.45	52.518	15.33
3.	250	1260.3	80.806	15.6

Table 4.8 Results of Flow Analysis for Swept Wing

	Velocity [m/s]	Lift [N]	Drag [N]	L/D
1.	150	423.84	31.04	13.65
2.	200	753.99	52.03	14.45
3.	250	1196.69	78.59	15.22

Table 4.9 Results of Flow Analysis for Plain Wing

	Velocity [m/s]	Lift [N]	Drag [N]	L/D
1.	150	480.81	35.72	13.45
2.	200	856.47	62.16	13.77
3.	250	1340.13	95.66	14.01

In this study, a new mechanism for the spanwise adaptive wing is designed. The proposed mechanism has two main features: Simplicity and reduced weight. The mechanism allows adjusting the wing in 2 DOF with one DOF at a time i.e., downwards or sideways. The use of Shape memory alloys makes the mechanism light in weight and enhances flight performance. The results obtained from the analysis of the wing in different forms conclude that morphing of the wing spanwise increases the lift-to-drag ratio. During the spanwise adaptive mode of bending the wing, at 250 m/s velocity and 0° angle of attack, the drag is reduced by 15.53% compared to the original wing configuration due to the gull shape of the wing. The overall lift-to-drag ratio is increased from 14.01 to 15.6. At the same time, for the same boundary conditions, the sweep mode of the wing reduces the drag by 17.84% and the

lift-to-drag ratio is increased from 14.01 to 15.22. Fig. 4.14 represents the plot of Lift versus velocity for spanwise adaptive wing, sweep wing and plain wing.

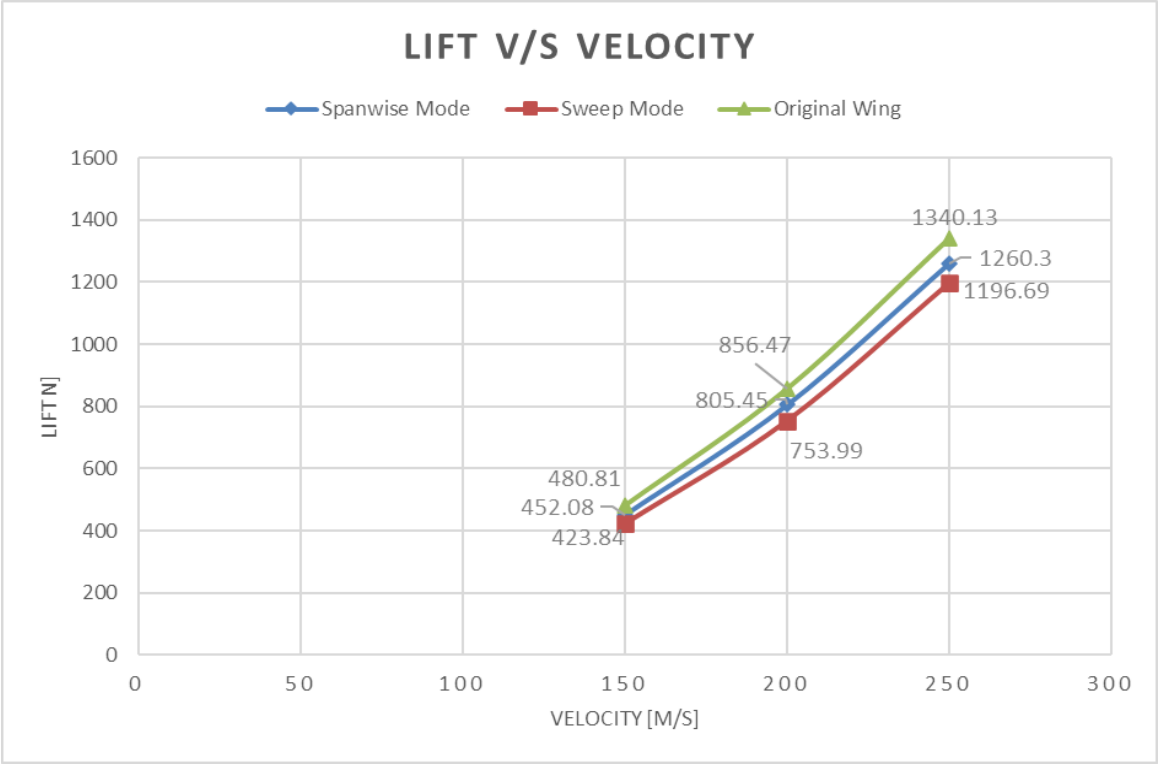

Fig. 4.14 A plot of lift vs velocity for spanwise, sweep and plain wing

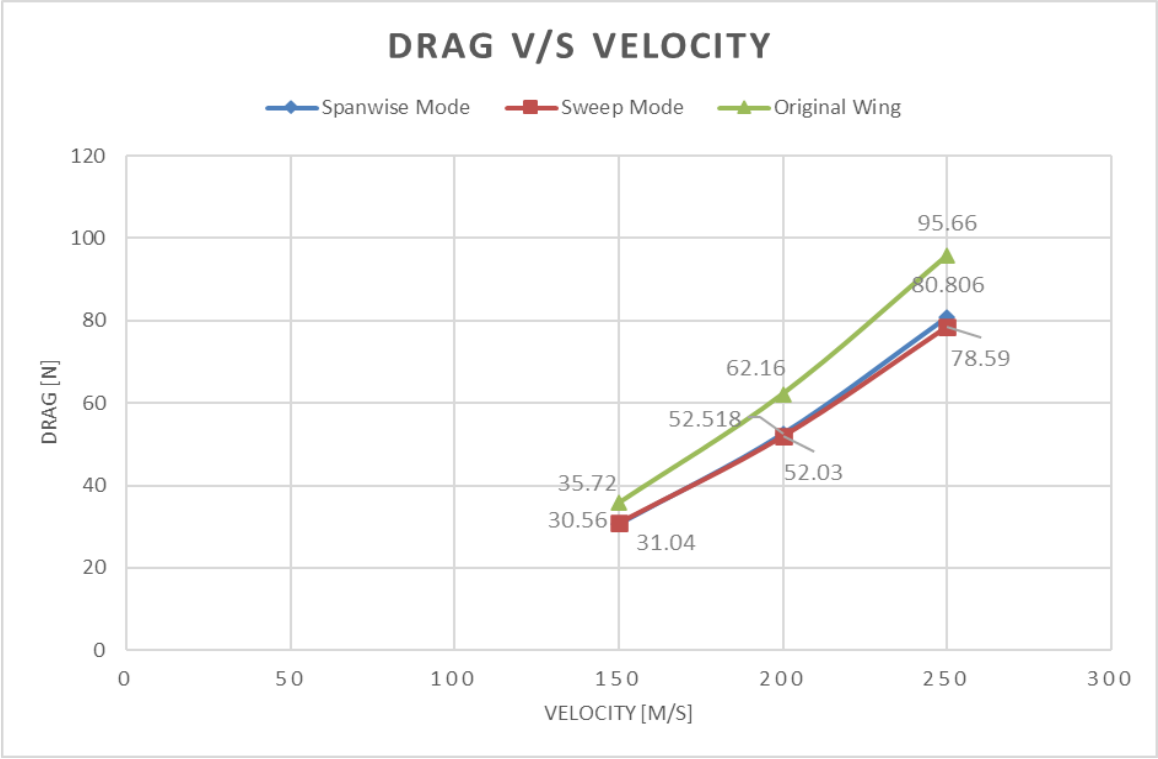

Fig. 4.15 A plot of drag vs velocity for spanwise, sweep and plain wing

Fig. 4.15 represents the plot of Drag versus velocity for spanwise adaptive wing, sweep wing and plain wing. Fig. 4.16 represents the plot of L/D versus velocity for spanwise adaptive wing, sweep wing and plain wing.

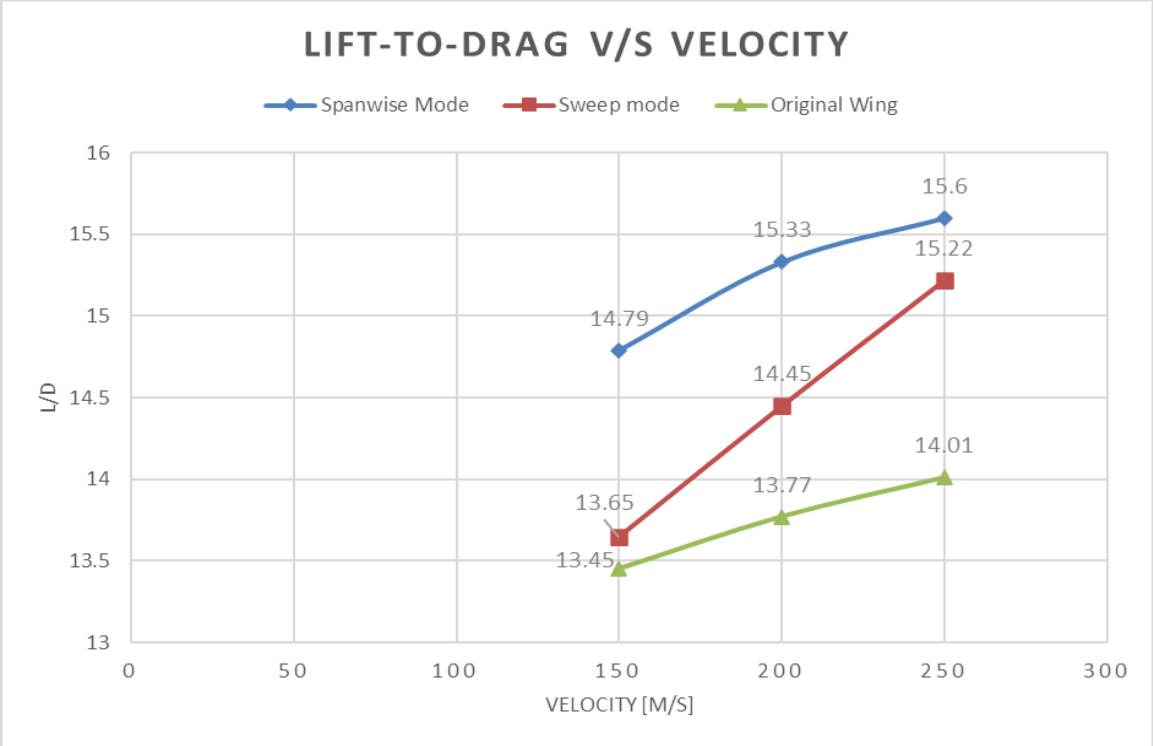

Fig. 4.16 A plot of L/D vs velocity for spanwise, sweep and plain wing

4.2.5 WING TRANSIENT ANALYSIS

The Spanwise adaptive model was analyzed by transient analysis and then compared with the original wing model to understand the characteristics with change in time. The transient analysis model had various system settings like:

- Step size: 0.01
- Total Number of Steps: 500
- Max Iteration: 20

Using these values and boundary conditions as 250 m/s velocity and 5% turbulence to match the atmospheric conditions. From the analysis, the results obtained with static analysis can be validated and at the same time the pressure contours over the wing at root and at the tip can be analyzed. The pressure contours at the root and tip for original wing remain constant with low pressure over the wing and high pressure under the wing. This means that the flow velocity is nearly same in spanwise direction.

For Spanwise Adaptive model, the wing which is bent at the tip has pressure higher than over the wing and lower pressure than under the wing when compared to original wing

which means the flow is not contributing towards the drag force. Thus, increasing the Lift-to-drag ratio (L/D).

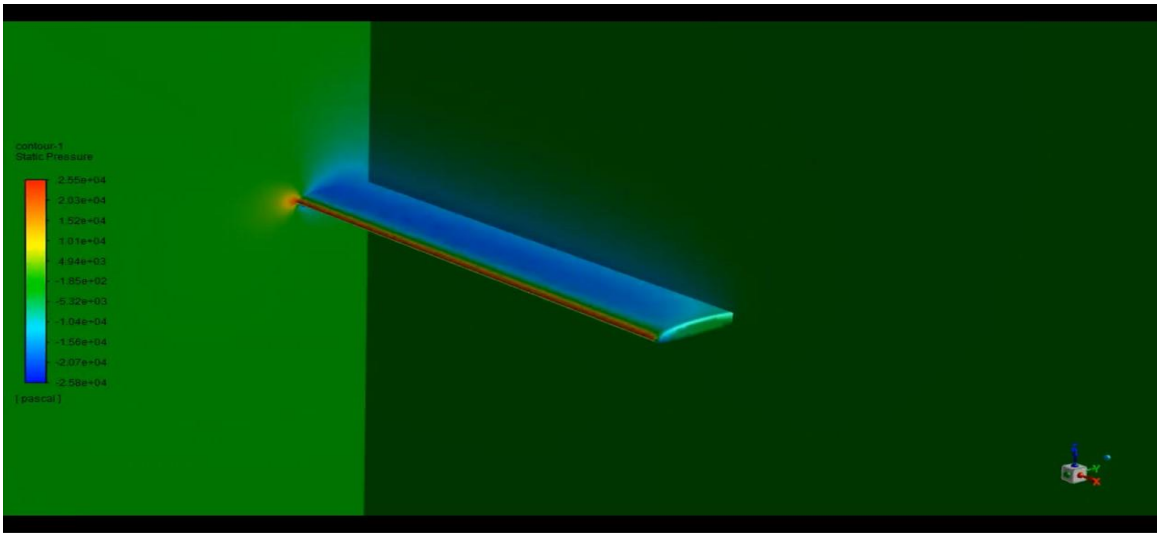

Fig. 4.17 Transient analysis over the plain and spanwise adaptive wing

CHAPTER 5

SUMMARY AND CONCLUSION

5.1 SUMMARY

A detailed study on the concept of Spanwise Adaptive Wing is done with the help of various literature papers and problem statements along with objectives have been identified. The selected airfoils were analyzed with XFLR and Ansys for accurate results. The grid independence study is made for the airfoils. After analyzing these airfoils at different speeds their lift and drag values were plotted for a different angle of attack and can be used to compare and finalize the airfoil using these criteria discussed for all three airfoils.

The model of the aircraft wing is modelled and the mechanism for using spanwise adaptive wing has been employed. Structural analysis is performed and finalization for the spar cross-section and material for the spar and ribs is done. Along with this modal analyses and flow analyses is performed for comparing this wing structure results with the spanwise adaptive wing.

5.1.1 AIRFOIL SELECTION

- The SD7037 airfoil has the best Lift values, low drag values, and greater stalling angle.
- Along with this, it has the best performance even at a greater speed which is matching with our problem statement.
- Based on this SD7037 airfoil has been selected.

5.1.2 WING MODELLING AND MATERIAL SELECTION FOR ANALYSIS

- Based on calculations and taking wing parameters in consideration the model of the wing is designed.
- The model with mechanism has been modeled.
- The model is tested for both I-section and C-section for the spar cross-section.
- The model is tested for 3 different materials and Aluminium 7075 T6 is chosen based on analysis.

5.1.3 ANALYSIS

- Static structural analysis is performed by considering factor of safety as 1.5.
- Modal analysis and transient analysis are performed.
- Flow analysis is performed for 150, 200 & 250 m/s for the wing and lift/drag plot has been plotted.

5.2 CONCLUSION

By observing the process and results obtained the outcomes and conclusion can be drawn. The drag reduction is visible as the use spanwise adaptive at higher subsonic speed is used. The comparison was made between plain wing, swept wing, and spanwise adaptive wing. The spanwise wing gives a higher lift to drag ratio and also drag is also reduced at these higher speeds. The use of this mechanism has helped to reduce the weight of the wing comparatively with various other mechanisms to reduce drag. The use of new material like shape memory alloy has made it possible to reduce this drag and also helps for easy production with just a spring. The use of spanwise adaptive wing with shape memory alloys has made it very easy to operate the mechanism and also provides good pressure and velocity distribution and avoiding hindrances to fly.

5.3 SCOPE FOR FURTHER WORK

The various further progress in this project can be made such as:

- Addition of high lift devices and various methods of heating or force applied to the shape memory alloy.
- Performing dynamic analyses, temperature-dependent study, and analyses, and performing vibrational analyses.
- Additional study concerning control surfaces and analyzing for greater stability and control of the wing.
- Fabrication of spanwise adaptive wing and test verify the results in wind turbines and structures lab.

PUBLICATIONS

[1] Butani Prince Nileshbhai, Kanagali Jayraj Pramod, Mahek Atul Sanghvi, Vinod Kumar Boyalla, Dr. Hareesha N G, "Articulation and Analysis of Spanwise Adaptive Wing", Journal of Huazhong University of Science and Technology, Volume 50, Issue 06, June-2021, ISSN: 1671-4512.

REFERENCES

[1] J. Yang, et al., "Dynamic Modeling and Flight Simulation of a Folding Wing-Tip UAV", 2020 Chinese Control and Decision Conference (CCDC), 2020, pp. 1814-1819, DOI: 10.1109/CCDC49329.2020.9164095.

[2] Fatima S, et al., "Articulation & analysis of span adaptive wing using wind tunnel", International Journal of Research and Review. 2018; 5(10):250-260.

[3] Benafan O., et al., "Recent Advancements in Rotary Shape Memory Alloy Actuators for Aeronautics", Shape Memory Super elasticity 5, 415–428 (2019). DOI: 10.1007/s40830-019-00260-3.

[4] Supekar, et al., "Design, analysis and development of a morphable wing structure for unmanned aerial vehicle performance augmentation." (2007).

[5] Çetin, et al., "Design of a UAV with Variable-Span Morphing Wing", University of Turkish Aeronautical Association, 06790, Ankara, TURKEY,2016, DOI:10.13140/RG.2.1.2185.1767/1.

[6] H. Basaeri, et al., "Experimental study of a bio-inspired robotic morphing wing mechanism actuated by shape memory alloy wires", Mechatronics, vol.24, issue.8, pp.2014-1231, DOI: 10.1016/j.mechatronics.2014.10.010.

[7] Bil C, et al., "Wing morphing control with shape memory alloy actuators", Journal of Intelligent Material Systems and Structures. 2013;24(7):879-898. DOI:10.1177/1045389X12471866.

[8] Sofla A. Y. N., et al., "Shape morphing of aircraft wing: Status and challenges", Materials & Design 31.3 (2010): 1284-1292.

[9] Mohd Jani, et al., "A review of shape memory alloy research, applications and opportunities", Materials & Design. 56. 1078-1113.DOI: 10.1016/j.matdes.2013.11.084.

[10] Darel E., et al., "Shape Memory Alloys, Properties and Selection Nonferrous Alloys and Special-Purpose Materials", Vol 2, ASM Handbook, By ASM Handbook Committee, ASM International, 1990, p 897–902, DOI: 10.31399/asm.hb.v02.a0001100.

[11] Ngo Khanh Hieu, et al., "Airfoil Selection for Fixed Wing of Small Unmanned Aerial Vehicles", Springer International Publishing Switzerland 2016.

[12] S. P. Venkatesan, et al., "Modelling and Analysis of Aircraft Wing with and Without Winglet", International Journal of Ambient Energy.

[13] Vasthadu, et al., "Vibrational Analysis Over an Aircraft Wing Section", International Journal of Advanced Science and Technology Vol. 29, No. 10s, (2020).

[14] Andersen, et al., "Aeroelastic Modeling, Analysis and Testing of a Morphing Wing Structure", 48th AIAA/ASME/ASCE/AHS/ASC Structures, Structural Dynamics, and Materials Conference.

[15] Arthur Rizzi, "Modeling and simulating aircraft stability and control—The simsac project", Progress in Aerospace Sciences, Volume 47, Issue 8,2011, Pages 573-588.

[16] Chung. P, et al., "Design, Manufacturing, and Flight Testing of an Experimental Flying Wing UAV", Applied Science 2019, 9, 3043.

[17] Ajith, et al., "Study of optimal design of spar beam for the wing of an aircraft", IJEDR, volume 5, issue 3, 2017.

[18] Shabeer KP, et al., "Optimization of aircraft wing with composite material", IJIRSET vol 2, Issue 6, June 2013, ISSN:2319-8753.

[19] Rajath Shetty, et al., "Design and fabrication of fixed wing UAV for air and underwater environments ", KSCST Project Reference No.: 42S_BE_1559.

[20] George N, et al., "The aircraft structural factor of safety", North Atlantic Treaty organization (advisory group for aeronautical research and development).

[21] http://airfoiltools.com/